



**Politecnico  
di Torino**

## **POLYTECHNIC OF TURIN**

Master's degree programme in Mechanical  
Engineering

A. Y. 2020/2021

October 2021

### ***Numerical investigation of the aero- thermal performance of a film cooling hole under several modelling assumptions***

**University supervisors:**

Chiar.ma Prof. Daniela Anna Misul  
Ing. Simone Salvadori  
Dr. Nicola Rosafio  
Chiar.mo Prof. Mirko Baratta

**Candidate:**

Samuele Renda

**Company supervisors:**

Ing. Daniele Coutandin  
Ing. Alberto Buonvino  
Ing. Mirko Pavan

Internship and thesis carried out at



## Table of Contents

<b>Abstract</b> .....	4
<b>List of figures</b> .....	5
<b>List of tables</b> .....	7
<b>Nomenclature</b> .....	8
<b>1. Introduction</b> .....	9
<b>2. Gas turbine working principle</b> .....	11
<b>2.1 Evolution of blade cooling and film cooling technology for HPT stages</b> .....	12
<b>2.2 Film cooling parameters</b> .....	15
<b>3 Computational Fluid Dynamics (CFD)</b> .....	28
<b>3.1 Introduction to CFD</b> .....	28
<b>3.2 Two equations turbulence models</b> .....	30
<b>3.3 CFD procedure</b> .....	31
<b>4 Test case description and pre-processing</b> .....	35
<b>5 mesh sensitivity analysis</b> .....	37
<b>6 Computational models and <math>\eta</math> results</b> .....	51
<b>6.1 Boundary conditions</b> .....	51
<b>6.2 Turbulence model comparison</b> .....	51
<b>6.3 Blowing ratio effect</b> .....	57
<b>6.4 Fillet radius effect</b> .....	61
<b>7 Discharge coefficient CD</b> .....	74
<b>8 Conclusions and future development</b> .....	76
<b>Acknowledgments</b> .....	79
<b>Ringraziamenti</b> .....	81
<b>References</b> .....	83

## Abstract

In gas turbines some parts are exposed to extremely high temperatures from the combustion gases well above the melting threshold of the material. Therefore, advanced cooling techniques are used to protect the parts exposed to these gases. One such system is the film cooling, necessary to guarantee a safe working condition for the turbine high-pressure stages. It consists in the ejection of cold air to maximize the coverage of an adiabatic layer of gas at lower temperature that protects the blade surface from the hot gas. A good prediction of the interaction between the mainstream and the coolant jet is important for the design of such advanced cooling system. A numerical study was conducted to investigate the behaviour of film cooling jet for a simple cylindrical hole on a flat plate. The numerical study was devoted to the assessment of different model parameters as well as mesh and geometrical features to be able to predict both the aerodynamic and thermal performance of the film cooling by means of Reynolds Averaged Navier-Stokes (RANS) approach. The case numerically studied was experimentally conducted at the University of Karlsruhe in the TATEF (Turbine Aero-Thermal External Flow) project. The goal of the project conducted at Karlsruhe aimed to reproduce the typical working conditions of a gas turbine stage. The numerical case study was analysed with adiabatic conditions, in this way the attention was focused on the film cooling effectiveness. The blowing ratio effect was analysed at three levels  $BR = 0.5$ ,  $BR = 1.0$  and  $BR = 1.5$ , combined with the effect of the turbulence model adopted, *standard  $k-\omega$* , *SST  $k-\omega$*  and *standard  $k-\varepsilon$* . Further investigation has been conducted in the end to study the effect of the fillet radius both at the channel inlet and outlet sections.

In general, all RANS models are not able to predict the mixing and consequently the distribution of coolant. The mixing between coolant and hot gas can be better resolved with models that are able to at least predict a fraction of the turbulence field.

## List of figures

Figure 1 Brayton-Joule cycle .....	11
Figure 2 Blade cooling evolution .....	13
Figure 3 Turbine vane cooling arrangement .....	14
Figure 4 Variation of blowing ratio .....	17
Figure 5 Effect of Density Ratio. DR=1.2 (top) DR=1.8 (bottom) .....	19
Figure 6 Effect of turbulence intensity .....	20
Figure 7 Characteristic dimension of a cylindrical hole .....	20
Figure 8 Effect of injection angle: $\alpha=60^\circ$ (top) $\alpha=90^\circ$ (bottom) .....	22
Figure 9 Effect of hole spacing: $s/D=3$ (top) $s/D=5$ (bottom) .....	23
Figure 10 Vortical structures .....	25
Figure 11 Simple cylindrical hole (left) and fan shaped hole (right) geometrical difference.....	25
Figure 12 Cylindrical hole with (top) and without upstream ramp (bottom) .....	26
Figure 13 Hole-in-slot geometry: mixing slot (top) shallow trench (bottom) .....	27
Figure 14 Computational domain .....	36
Figure 15 Fillet geometry .....	36
Figure 16 Detail of polyhedral mesh from converted tetrahedral grid.....	38
Figure 17 Local effectiveness BR=1.0 Tetrahedral Coarse mesh (top), Intermediate mesh, Fine mesh, Ultrafine mesh (bottom) .....	39
Figure 18 Local effectiveness BR=1.0 Polyhedral Intermediate mesh (top), Fine mesh, Ultrafine mesh (bottom) .....	40
Figure 19 Laterally averaged effectiveness BR=1.0 Comparison between tetrahedral and polyhedral mesh.....	41
Figure 20 Mach number sections perpendicular to the channel axis: Tetrahedral (left) Polyhedral (right) .....	42
Figure 21 Symmetry plane Mach number in the channel: Tetrahedral (top) Polyhedral (bottom).....	42
Figure 22 Symmetry plane velocity vectors: Tetrahedral (top) Polyhedral (bottom) .....	44
Figure 23 Velocity magnitude at the inlet hole. Extension of the recirculation for the polyhedral solution (bottom) .....	44
Figure 24 Symmetry plane velocity vectors: addition of the production limiter. Tetrahedral (top) Polyhedral (bottom).....	46
Figure 25 Mach number in the channel: addition of the production limiter. Tetrahedral (top) Polyhedral (bottom) .....	47
Figure 26 Mach channel sections perpendicular to the channel axis: addition of the production limiter. Tetrahedral (left) Polyhedral (right).....	47
Figure 27 Local and laterally averaged effectiveness compared to experimental results.....	48

Figure 28 Computational domain mesh .....	49
Figure 29 Channel mesh.....	49
Figure 30 Cooled surface mesh .....	50
Figure 31 Fillet channel-plenum mesh: sharp edge, 1.25%D, 2.5%D, 3.75%D, 5%D, 7.5%D, 10%D, 15%D (from left to right, top to bottom) ...	50
Figure 32 Comparison of $\eta_{lat}$ at different turbulence model and geometrical channel edges .....	53
Figure 33 Corresponding $\eta_{aw}$ of Figure 32.....	54
Figure 34 Mach number inside the channel. Sharp edge solutions (left) and filleted solutions (right) .....	55
Figure 35 Mach number k- $\omega$ , sharp edge (top) and fillet (bottom) .....	56
Figure 36 Mach number SST k- $\omega$ , sharp edge (top) and fillet (bottom) ...	56
Figure 37 Mach number k- $\epsilon$ , sharp edge (top) and fillet (bottom) .....	57
Figure 38 $\eta_{lat}$ at BR=0.5, BR=1.0 and BR=1.5 .....	58
Figure 39 $\eta_{aw}$ BR=0.5 comparing experiment (top), SST k - $\omega$ (middle) and k - $\epsilon$ (bottom) .....	58
Figure 40 $\eta_{aw}$ BR=1.0 comparing experiment (top), SST k - $\omega$ (middle) and k - $\epsilon$ (bottom) .....	59
Figure 41 $\eta_{aw}$ BR=1.5 comparing experiment (top), SST k - $\omega$ (middle) and k - $\epsilon$ (bottom) .....	59
Figure 42 Mach number channel sections .....	60
Figure 43 Laterally averaged effectiveness BR=0.5 .....	63
Figure 44 Local adiabatic effectiveness BR=0.5 .....	64
Figure 45 Mach number inside the hole at BR=0.5.....	65
Figure 46 Mach number inside the hole at BR=1.0 .....	65
Figure 47 Laterally averaged effectiveness BR=1.0 .....	66
Figure 48 Local adiabatic effectiveness BR=1.0 .....	67
Figure 49 Laterally averaged effectiveness BR=1.5 .....	68
Figure 50 Local adiabatic effectiveness BR=1.5 .....	69
Figure 51 Mach number inside the hole at BR=1.5 .....	70
Figure 52 Mach number at BR=1.0 for sharp edge (top), 5% radius (middle) and 15% radius (bottom).....	71
Figure 53 Discharge coefficient.....	75

## List of tables

Table 1 Main variables affecting film cooling performance .....	16
Table 2 Test matrix definition .....	34
Table 3 Mesh parameters .....	37
Table 4 Boundary conditions.....	51
Table 5 Blowing ratios at different fillet radius conditions.....	73
Table 6 Discharge coefficients.....	75

## Nomenclature

$BR$	Blowing ratio
$CD$	Discharge coefficient
$D$	Channel diameter
$Ma$	Mach number
$P$	Pressure
$R$	Fillet radius
$T$	Temperature
$v$	Velocity
$\gamma$	Heat capacity ratio
$\rho$	Density
$\eta$	Film cooling effectiveness

## Subscripts

$aw$	Adiabatic wall
$c$	Coolant
$is$	Isentropic
$lat$	Laterally averaged
$m$	Main flow
$rec$	Recovery
$0$	Total

## **1. Introduction**

The following project is the result of the collaboration between Polytechnic of Turin and Avio Aero, a world leadership company in the aviation industry, with headquarter in Rivalta di Torino, as well as many other plants throughout Italy and Europe. Avio Aero is a GE Aviation business, it operates in the design, manufacture and maintenance of civil and military aeronautics systems and subsystems, from the product design and development through the production and to the aftermarket.

High Pressure Turbine (HPT) stages are exposed to high inlet temperatures that most likely overcome the melting temperature limit of the materials. The efficiency and power output of a gas turbine can be improved by increasing the inlet temperature that can exceed 2000°K nowadays and will tend to be higher and higher. For this reason advanced cooling technology plays a major role in the development of gas turbine engines to ensure safe operating conditions of high pressure stages.

The project carried out has the goal to study the external cooling system of the blades of the High Pressure Turbine stages. External cooling strategies are better known as film cooling and it is achieved by bleeding compressed air at lower temperature by means of external cooling holes on the blade surface, which eject coolant from internal passages and create a film that insulates the blade surface. Even though it protects the machine, it consumes compressed air, because it is spilled from the compressor stages, and it negatively influences the performance in particular when the coolant penetrates in the main flow. Therefore, extensive research is needed to improve film cooling efficiency.

During the development of the final thesis, the work has been focused on studying the film cooling effectiveness which is used to quantify how well the coolant is covering the surface, meaning how well it is protecting the blade surface.

This project has the goal to analyse and study both the thermal and aerodynamic performance of film cooling on a flat plate, aiming at finding

what are the effects of different numerical setups as well as different geometrical characteristics, considering a cylindrical cooling channel.

The macro steps that will be presented in this thesis are listed right away.

- To help in the introduction of this subject a brief explanation on the working principle of a gas turbine is added to ease the reader in a better understanding of the phenomena that happen inside a gas turbine engine.
- Following up, an introduction on the film cooling, describing what are the main parameters, either geometrical or fluid properties, that influence its performance, reducing or increasing it, based on open literature results.
- Once introduced a background on the film cooling and a brief explanation on the working cycle of a gas turbine, the steps done to reach the conclusions of this project will be explained:
  - the creation of the 3D computational domain;
  - the meshes generation;
  - the numerical implementation in the Computational Fluid Dynamics (CFD) program;
  - the post-processing and discussion of the results.

To have a better understanding of the numerical solutions, the results are compared with experimental data from the TATEF (Turbine Aero-Thermal External Flow) [1-2]. This data provides an extensive set of solutions covering all aspects related to the film cooling, such as discharge coefficient, laterally averaged effectiveness, turbulence intensity effects, interaction of film cooling rows and wake passing on film cooling. However, for the purpose of the thesis, only laterally averaged data and discharge coefficient are considered as a check.

In conclusion, the results obtained will be summarised, offering suggestions for the future development based on the results obtained and possible improvement that can be done, also considering what has already been done in literature.

## 2. Gas turbine working principle

Gas turbines are used in many fields of engineering, from aircraft propulsion to power plant generation. Such a machine is a very delicate and complex structure that represents a challenge in the engineering field, demanding more and more energy, maximizing the efficiency and at the same time reducing the environmental impact. It is a very complex machine, yet at the same time very easy to understand its working principle. The whole structure can be divided in three main sections: the compressor, the combustion chamber, and the turbine in the outlet portion of the engine. This machine works with ambient air and its working conditions are identified by means of a cycle called *Brayton-Joule cycle* shown in Figure 1. The black lines represent the ideal cycle, whereas the blue lines are the real cycle characterized by the irreversibility of the engine.

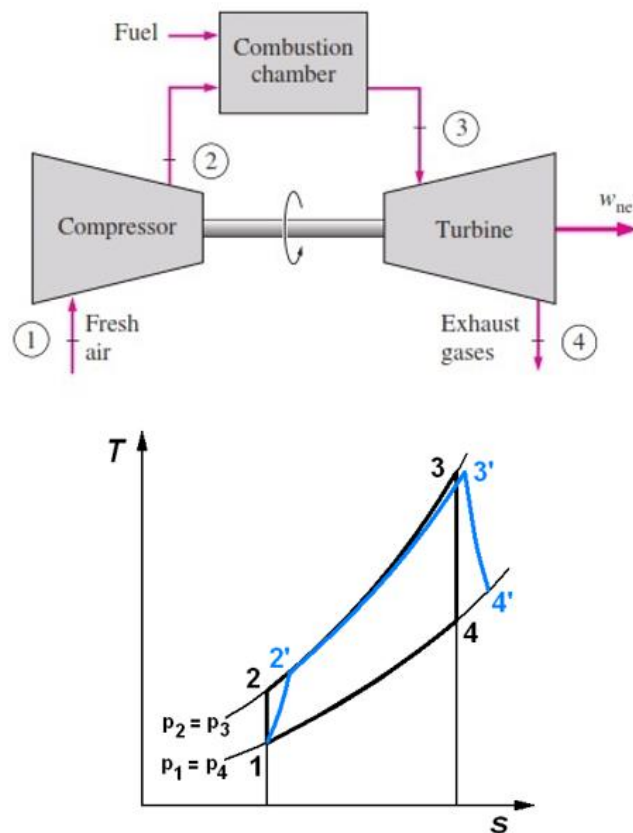


Figure 1 Brayton-Joule cycle

Air is demanded by the compressor (1) and is being compressed (1→2) increasing its temperature and pressure; fuel is added to fairly hot air in the burner to originate a combustion and reaching high temperature (3), following an almost isobaric process; the high temperature gas is then expanded through the turbine stages (3→4), generating power for the engine to produce the thrust necessary in the exit nozzle and the work that drives the compressor.

Maximum temperature and pressure are the two important parameters necessary to obtain engines' performance as high as possible in terms of efficiency and power output. They increase with increment in turbine inlet temperature. To obtain this goal an important issue has to be taken into consideration: the temperature threshold the material itself can sustain. Nowadays turbine inlet temperature is much higher than what the material could sustain, with temperatures that can exceed 2000°K, for this reason an advanced and efficient cooling system is required, that enables the engine to work in a safe operative condition.

## **2.1 Evolution of blade cooling and film cooling technology for HPT stages**

Due to the high temperature from the hot combustion gases, more and more research on innovative materials is done to find materials that can exhibit high thermo-mechanical properties with the ability to preserve the mechanical characteristics with the increase in temperature, without neglecting other important properties such as corrosion.

Even though over the past decades there has been an improvement on the material used, this is still not sufficient to resist to the thermal stresses the materials are subjected. For this reason complex cooling systems have been added to solve this problem. The following figure (Figure [2](#)) gives a perspective on the evolution of blade cooling.

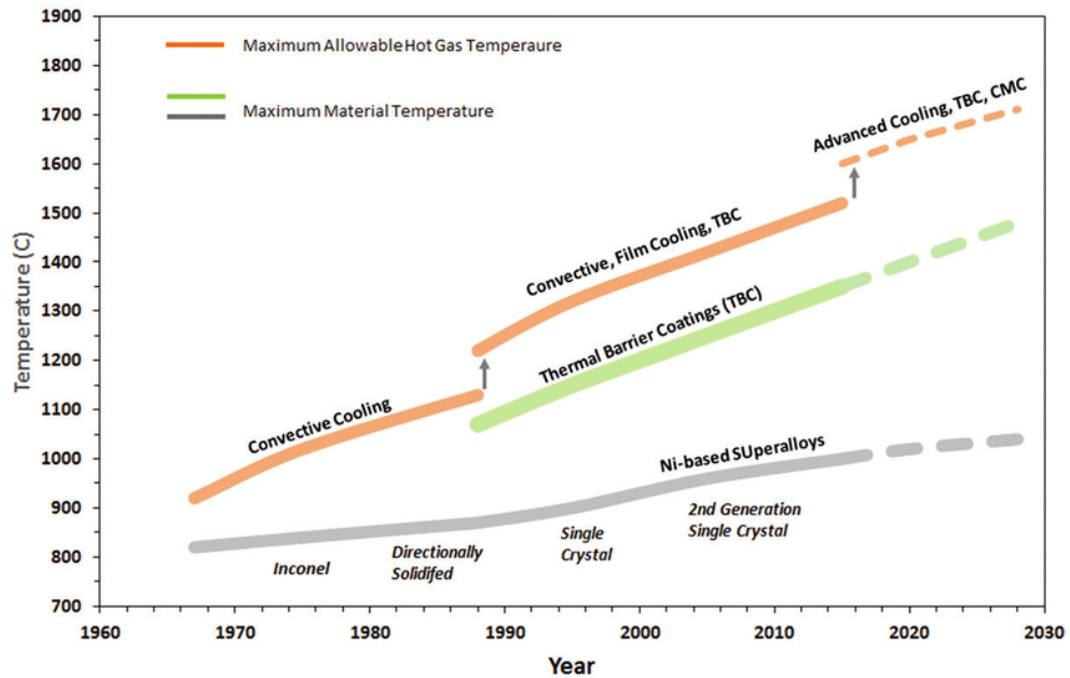


Figure 2 Blade cooling evolution

As can be seen from the graph the research on materials have brought to an increase in temperature resistance for Ni-based alloys, depending on the internal structure of the material itself. With the use of particular coating solutions combined with effective cooling solutions, the temperature limit sustained by the materials has increased drastically and will continue to increase with extensive investigations. With the adoption of this technology the admissible temperature has passed from a mere  $\sim 920^{\circ}\text{C}$  ( $\sim 1200^{\circ}\text{K}$ ) up to  $\sim 1700^{\circ}\text{C}$  ( $\sim 2000^{\circ}\text{K}$ ) in the next years.

Typically, the blade cooling is applied to the first stages of the turbine, the so called High Pressure Turbine (HPT), which is the part directly exposed to the hot combustion gases. This technology is classified in internal and external cooling. External cooling is better known as film cooling, where internal coolant air is ejected through holes or slots to create an adiabatic layer of coolant on the surface to protect the blade from the combustion gases. Cold air used for cooling is drawn from the first stages of the compressor, resulting in losses in the engine efficiency.

Film cooling technology is the most efficient and advanced cooling system known up until now, but this technique is very complex both from a physical

point of view due to the fluid-dynamic complexity in the interaction between coolant and hot gas, and from a modelling standpoint since the complexity of the mixing results in difficult prediction and modelling due to the modifications based on the different thermodynamics parameters. In order to create a good protective film, hence a high cooling efficiency, it is necessary that there is a continuous action of the coolant, thus create a film that does not vanish as the hot gas passes but form a permanent protective layer. As consequence, it is necessary that during the design operation a proper injection mechanism is foreseen, modifying accordingly the geometry of the holes throughout the blade surface. A scheme of the cooling arrangement of a blade is reported in the following figure (Figure 3).

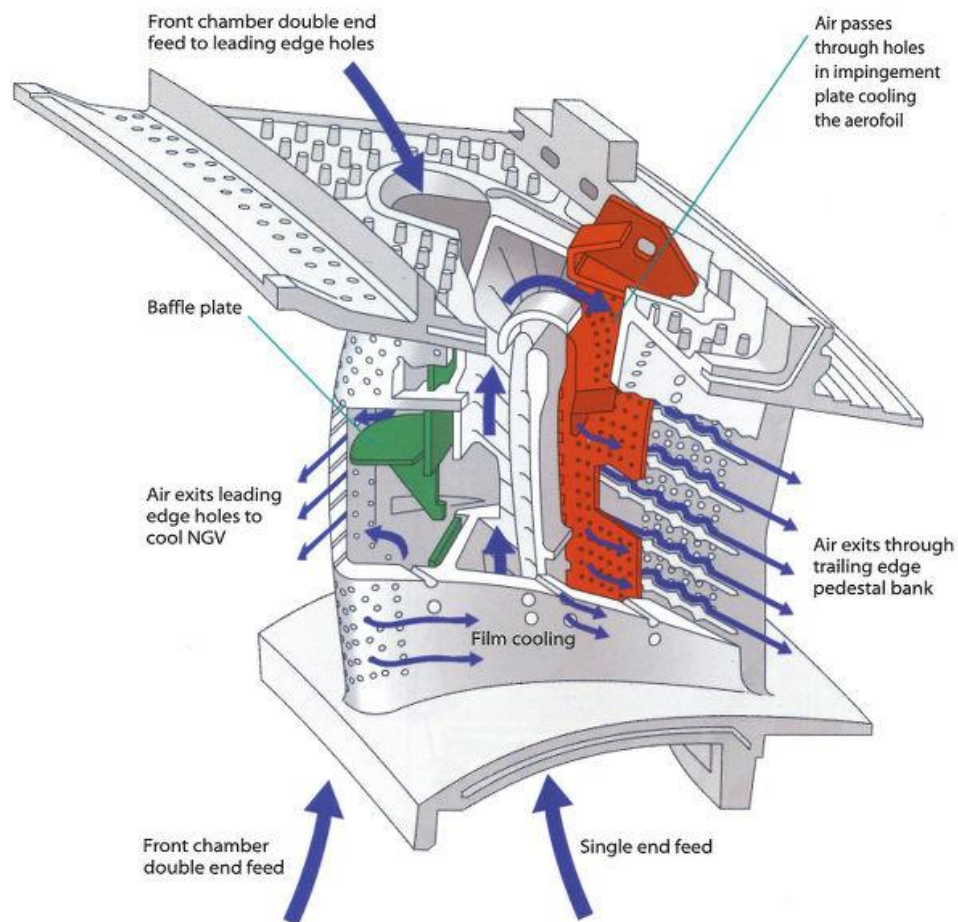


Figure 3 Turbine vane cooling arrangement

## 2.2 Film cooling parameters

Cooling through film cooling is a complex mechanism, affected by many parameters related to hole geometry, development of the coolant flow through the hole, and the mainstream above the surface of interest. Tools for prediction and comparison of film cooling performance are essential. As the film cooling interacts with the main flow, its performance is defined by the adiabatic film cooling effectiveness (1) [3], where  $T_{aw}$  is the adiabatic wall temperature,  $T_{rec,m}$  (2) is the mainstream recovery temperature, and  $T_{0c}$  is the total coolant temperature.

$$\eta_{aw} = \frac{T_{aw} - T_{rec,m}}{T_{0c} - T_{rec,m}} \quad (1)$$

$$T_{rec,m} = T_{0m} \frac{1 + \text{Pr}^{0.33} \frac{\gamma - 1}{2} Ma_{is}^2}{1 + \frac{\gamma - 1}{2} Ma_{is}^2} \quad (2)$$

Since the coolant interacts with the hot gas, usually the NHFR (Net Heat Flux Reduction) is calculated (3). This parameters allows to measure the performance of the film cooling to reduce the heat flux to the wall, comparing the heat flux with film cooling to the local heat flux that would occur without film cooling. In principle, the heat transfer on a cooled surface is higher than the heat transfer of an uncooled case.

$$NHFR = 1 - \frac{q_f}{q_0} = 1 - \frac{h_f}{h_0} \left( 1 - \frac{\eta_{aw}}{\phi} \right) \quad (3)$$

$\eta_{aw}$  and  $NHFR$  are not the only non-dimensional parameters to investigate in the film cooling performance. The Discharge Coefficient  $CD$  (4) allows to measure the irrecoverable losses of the fluid in the channel, mainly caused by the separation of the flow at the inlet section.

$$CD = \frac{\dot{m}_c}{p_{0c} \left( \frac{p_m}{p_{0c}} \right)^{\frac{\gamma+1}{2\gamma}} \left( \frac{2\gamma}{(\gamma-1)RT_{0c}} \left( \left( \frac{p_{0c}}{p_m} \right)^{\frac{\gamma-1}{\gamma}} - 1 \right) \right)^{1/2}} \frac{\pi D^2}{4} \quad (4)$$

The non-dimensional parameters allow to analyse the results at various operating conditions, enabling to draw conclusions on the solutions. However, a good understanding and investigation of the variables that

influence the film cooling performance is what truly allow to understand those results. Many are the variables affecting the film cooling performance and countless is the combination of these variables to affect the coolant layer. For this reason, in Table 1 a series of geometrical and fluid-dynamic variables are presented to give a literature review of their effects.

Geometrical	Fluid-dynamic
Ejection angle $\alpha$	Blowing ratio <b>BR</b>
Hole spacing <b>s</b>	Density ratio <b>DR</b>
Channel length <b>L</b>	Turbulence intensity <b>Tu</b>
Downstream distance <b>x</b>	

*Table 1 Main variables affecting film cooling performance*

Baldauf et al. [4] investigated what is the effect of the main parameters on the film cooling performance, attempting to describe film cooling by means of a correlation. Study on flat plate film cooling gives a perception of the various parametric effects under engine-like conditions.

$$\bar{\eta} = f\left(BR, DR, Tu, \alpha, \frac{s}{D}, \frac{L}{D}, \frac{x}{D}\right) \quad (5)$$

## **FLUID-DYNAMIC PROPERTIES**

- **Effect of blowing ratio BR:** blowing ratio is the measure of how much the coolant is ejected to create the protective layer. Blowing ratio is measured as the ratio between density and velocity of the coolant over those of the mainstream.

$$BR = \frac{\rho_c v_c}{\rho_m v_m} \quad (6)$$

Figure 4 shows the effect the variation in blowing ratio has on the laterally averaged effectiveness.

At very low values of blowing ratios the cold air spreads on the blade surface immediately at the hole exit. For this reason the curves present a high effectiveness peak value almost in correspondence of the trailing edge of the exit hole. The coolant jet is rapidly mixed with

the mainstream due to its low velocity, therefore the film cooling performance presents a fast decay in film cooling effectiveness.

Increasing the blowing ratios to moderate values the effectiveness peak tends to move downstream since the jet requires some downstream distance to distribute on the surface. The overall effectiveness increases due to the increase in mass flow rate that reduces the film cooling temperature rise. However, an increase in blowing ratio starts lifting off the coolant jet from the surface, resulting in hot gas to pass underneath the coolant jet. Consequently, this leads to a decrease in the effectiveness peak, even though the jet lifting off does not outweigh the beneficial effect of the protective film yet for low and moderate blowing ratios.

Moving to high blowing ratios, the overall trend of the curve is changed. The decay characteristic downstream from the hole is lost and the effectiveness peak is no more evident, the curve rather tends to stabilize at a constant value of laterally averaged effectiveness. Jet lift-off is considerably present, strong coolant momentum enables the jet to penetrate in the mainstream resulting in an overall decrease of the effectiveness.

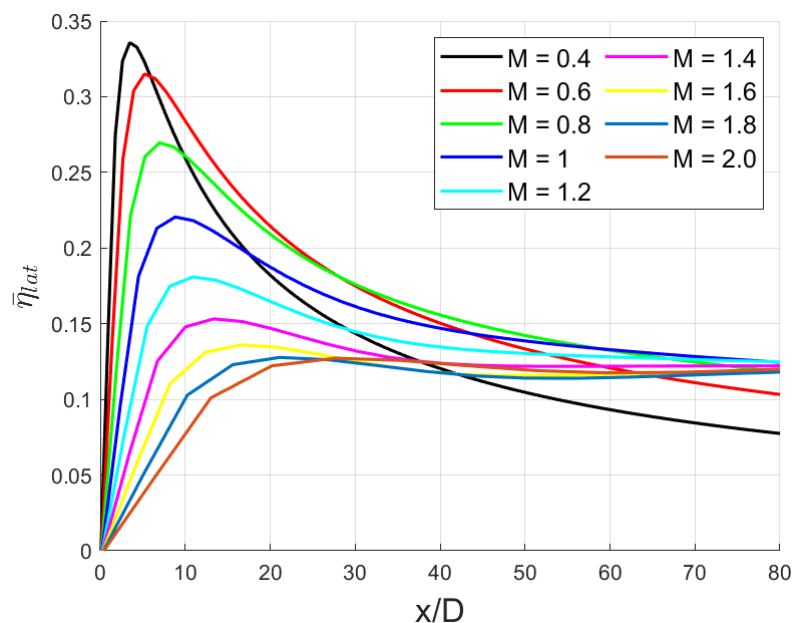


Figure 4 Variation of blowing ratio

To the blowing ratio there is also another variable that influence the film cooling performance, and that is the *Momentum Flux Ratio MR*.

$$MR = \frac{\rho_c v_c^2}{\rho_m v_m^2} = \frac{BR^2}{DR} \quad (7)$$

Both blowing ratio and momentum flux ratio have been used to scale results. Baldauf et al. investigated the scaling with both variables. Their studied proved that scaling using the blowing ratio gives good prediction far downstream the hole, showing a common decay trend of the effectiveness, while scaling with the momentum flux ratio the opposite happen, that is to say good results are obtained for short downstream distances.

- **Density ratio effect DR:** Figure 5 shows results at low and high density in the same blowing ratio range as in Figure 4.

The same trend of the laterally averaged effectiveness curves can be observed: high peaks and fast decay for low blowing ratios and lower effectiveness peaks converging to constant values increasing the blowing rate.

The impact of the high density ratio is not obvious until a closer inspection of the curves is made. Generally, at a given blowing ratio value, higher density ratio gives higher film cooling effectiveness. This can be justified since the resulting momentum of the coolant jet is lower, in this way the main flow can push down the jet creating a better coolant layer and ultimately resulting in lower tendency of the jet to lift off.

The study conducted by Baldauf et al. found that at lower density ratio the peak effectiveness is reduced, but at the same time also the blowing ratio at which that level is reached is reduced. In conclusion, being that this overall effectiveness is obtained at different blowing ratios, a lower density ratio can be used so to obtain the same overall effectiveness but with less amount of coolant.

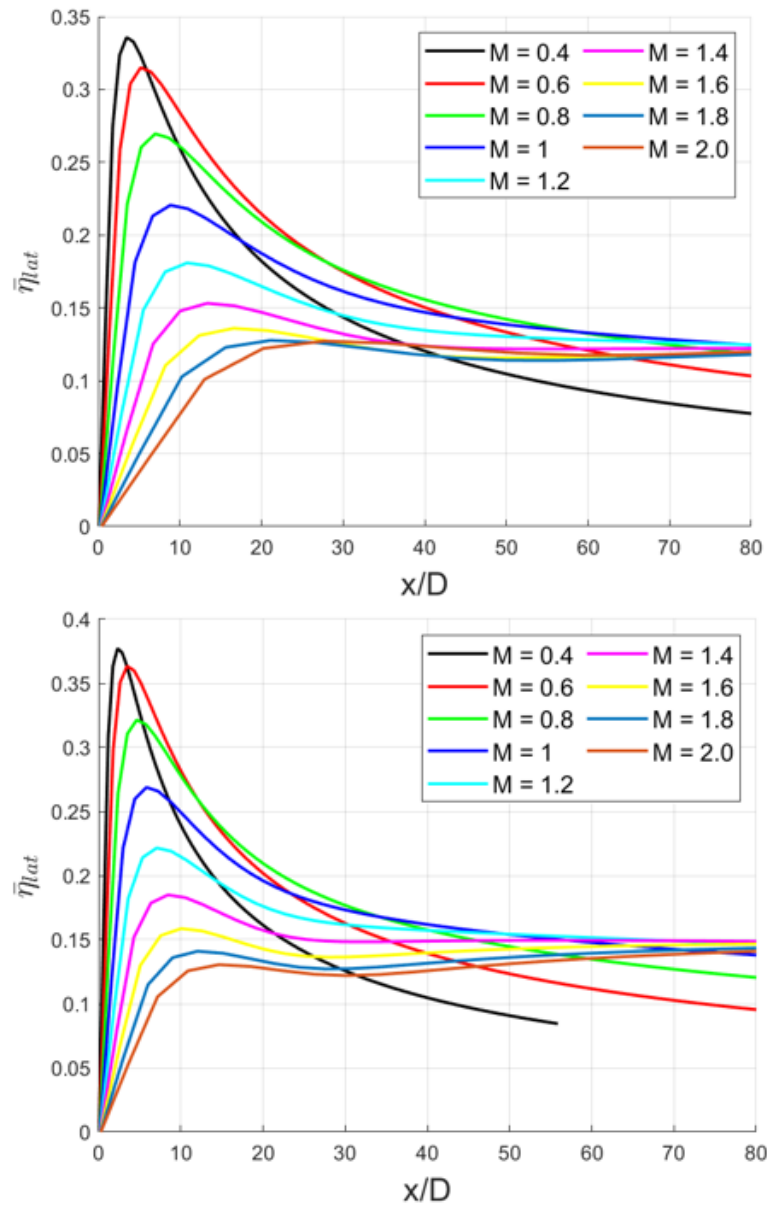


Figure 5 Effect of Density Ratio. DR=1.2 (top) DR=1.8 (bottom)

- Effect of mainstream turbulence intensity  $Tu$ :** Figure 6 shows a comparison of three levels of turbulence at three levels of blowing ratio, representing low, moderate and high condition. Close to the ejection position Baldauf et al. concluded that at low blowing ratio the effectiveness peaks are higher at high turbulence level because the increased turbulence level promotes the coolant mixing, hence increasing jet spreading close to the hole outlet. Far downstream, where the flow is dominated by the turbulence effect, an increased

mixing at elevated turbulence values causes an effectiveness reduction for all blowing ratios. This effect is more evident at lower level of blowing ratio, where the turbulence from the exiting coolant jet is low, introducing an important effectiveness loss.

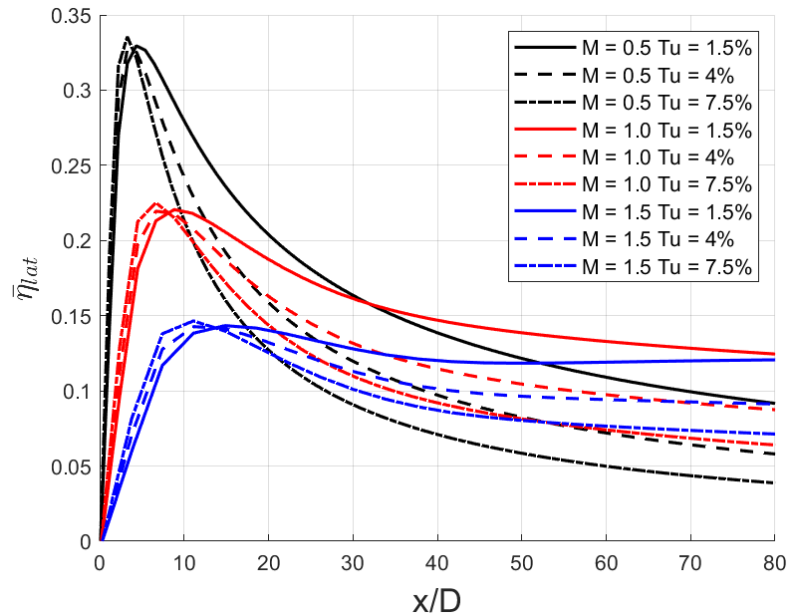


Figure 6 Effect of turbulence intensity

## GEOMETRIC PROPERTIES

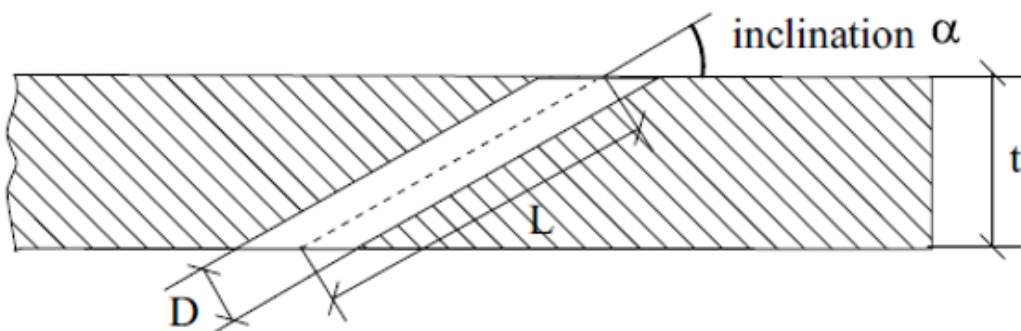


Figure 7 Characteristic dimension of a cylindrical hole

- **Effect of ejection angle  $\alpha$ :** hole inclination with respect to the hot gas stream is very important for film cooling performance when it comes to penetration of the coolant and coverage of the coolant over

the blade surface. Figure 8 shows the effect of the injection angle of  $60^\circ$  and  $90^\circ$ . A shallow injection angle (Figure 4) reduces the separation of the jet from the wall, therefore increasing film cooling effectiveness. The only issue with a very shallow angle is the manufacturing of it, there might be problems with the machining. Compared with a steeper ejection angle, the peak effectiveness downstream the hole can be reached with lower blowing ratio, hence less mass flow rate is required, but the effectiveness declines faster. Moreover, steeper angle enhances adjacent jet interaction at higher blowing ratios, resulting in higher overall effectiveness compared to more shallow ejection angles.

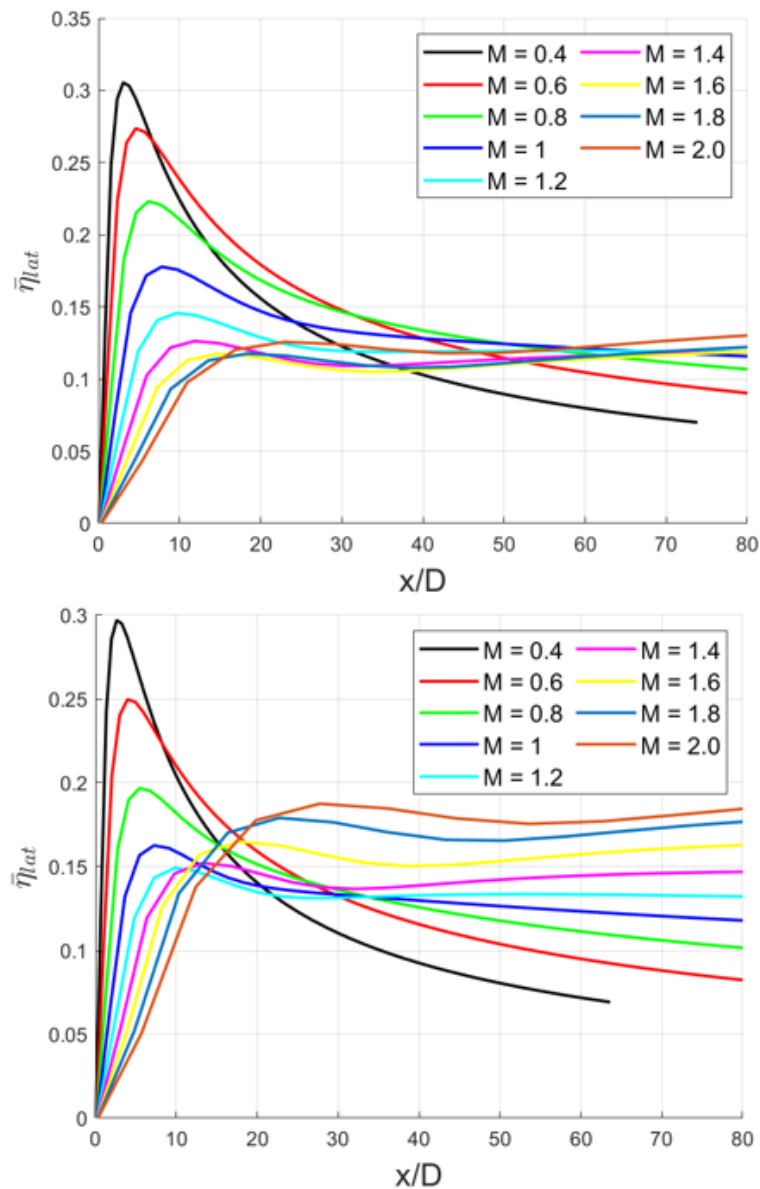


Figure 8 Effect of injection angle:  $\alpha=60^\circ$  (top)  $\alpha=90^\circ$  (bottom)

- Effect of hole spacing  $s/D$ :** Figure 9 shows the effect of the pitch between holes on the laterally averaged effectiveness. At a small hole spacing the laterally averaged effectiveness is much more above the values achieved at increased hole spacing, due to an increased amount of coolant per surface area. Baldauf et al. found out that closer holes result in an increased influence from adjacent jet interaction, while a wider space results in more single jet in cross-

flow effect. For large hole spacing they discovered that there is no influence from the adjacent jet interaction.

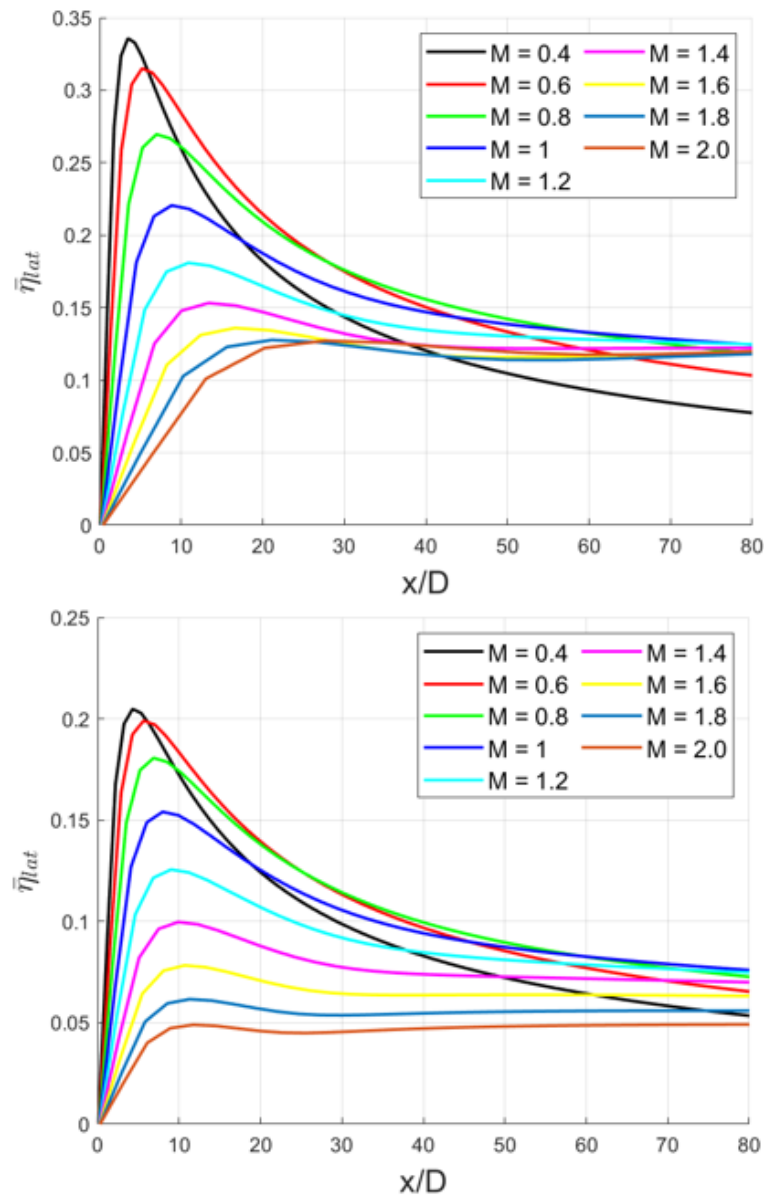


Figure 9 Effect of hole spacing:  $s/D=3$  (top)  $s/D=5$  (bottom)

- Hole length effect  $L/D$ :** Lutum and Johnson [5] conducted a study to investigate the effects of channel length-to-diameter ratio on the film cooling effectiveness. The results showed that for hole length greater than five times the diameter no significant changes in the effectiveness distribution were observed, the coolant flow inside the

cylindrical hole was established after five hole diameters. They studied  $L/D$  from 1.75 to 18 and length-to-diameter ratio shorter than 5 resulted in lower film cooling effectiveness. The difference in effectiveness obtained between short and long holes increased with blowing ratio. The difference is explained by Lutum and Johnson: the flow inside the hole is not able to fully develop for short hole length, once the flow is completely developed it will not change whether the length is further increased; another possible explanation of this phenomenon is explained and it is due to the greater effective ejection angle that is obtained, coming from the undeveloped flow in the channel that does not have time to align properly with the direction of the hole.

- **Downstream distance  $x/D$ :** downstream distance is an essential parameter and most of the time the graphs are plotted in function of this variable. Hence, the graphs show how the film cooling effectiveness changes along the downstream surface of the outlet hole.

The main geometrical and fluid-dynamic variables affecting the film cooling performance have been introduced, giving a general idea on how the film cooling effectiveness behaves at different conditions. However, it is good to give a more detailed explanation of the phenomenon. Fundamental flow dynamics is very important, good prediction and understanding of the interaction between coolant jet and hot gas freestream is what enables to obtain good results of the simulations. The interaction of the jet and the mainstream result in complex vortical structures. Zhang et al. [6] presented a study, investigating the formation of these vortexes, as displayed in Figure 10, and their effect of the coolant jet.

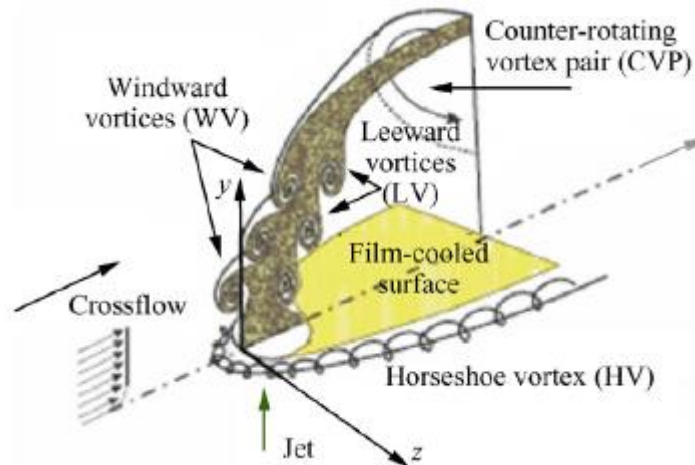


Figure 10 Vortical structures

Four main vortical structures are formed from the mutual interaction of coolant jet and main flow: Windward Vortices (WV), Counter-rotating Vortex Pair (CVP) denoted also as kidney vortices for their shape, Horseshoe Vortices (HV), and Leeward Vortices (LV).

According to Zhang et al. the CVP is the dominant flow mechanism that affect the film cooling since this vortex structure makes the coolant jet to lift and go above the surface. Accordingly, in order to enhance film cooling performance it is necessary to find ways to reduce these specific vortices. Changing the channel geometry into shaped holes is one of the most promising way to achieve this result. Shaped holes give better results when compared to simple cylindrical holes, with less penetration of the coolant jet into the mainstream and better lateral coverage.

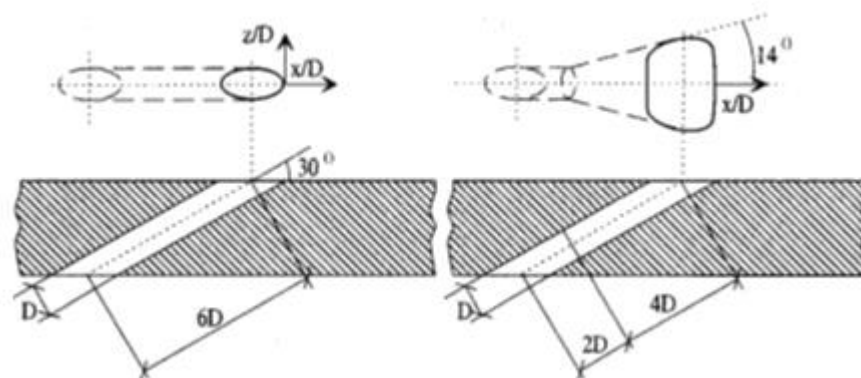


Figure 11 Simple cylindrical hole (left) and fan shaped hole (right) geometrical difference

Zhang et al. presented in their investigation innovative ways to deal with Counter-rotating Vortex Pair and enhance as much as possible the film cooling performance, such as optimized shaped hole geometries, ramps upstream the exit section of the hole (Figure 12) made to create a controlled recirculation region to reduce the static pressure ahead of the hole exit and thus increase the lateral distribution of the coolant, holes inside a slot (Figure 13) in order to allow the premixing and then exit as a slot-like jet, and active solutions like pulsed film cooling or the use of plasma actuators. The solutions presented and investigated by Zhang et al. result in an improvement of the film cooling, but nowadays these solutions may not be feasible due to the complexity in their fabrication, but in the future these may result in advanced systems that will help to further increase the film cooling performance.

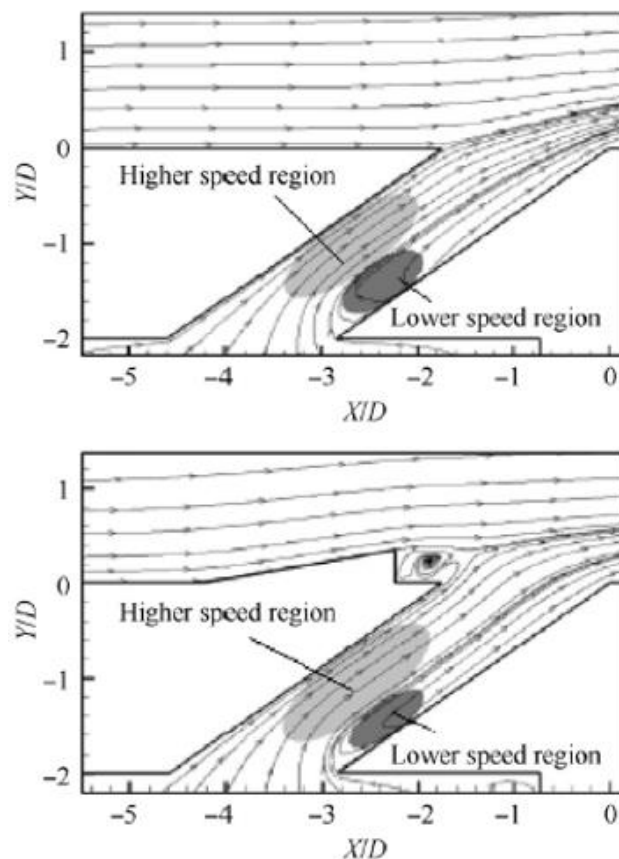


Figure 12 Cylindrical hole with (top) and without upstream ramp (bottom)

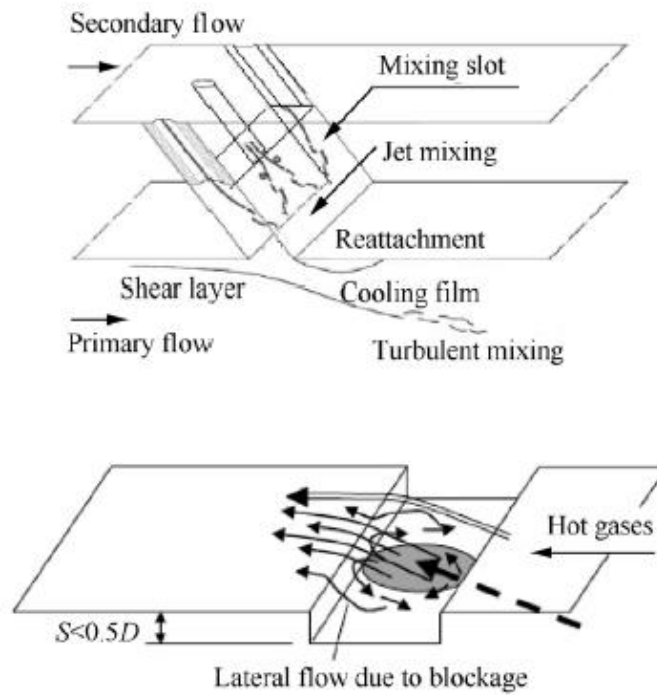


Figure 13 Hole-in-slot geometry: mixing slot (top) shallow trench (bottom)

## 3 Computational Fluid Dynamics (CFD)

### 3.1 Introduction to CFD

Computational Fluid Dynamics is a tool that uses algorithms to simulate and solve fluid-dynamic problems. It is used in industries to investigate all the problems related to fluids. For the investigation carried out for this project, ANSYS Fluent has been used.

The basis of the simulations is to solve the Navier-Stokes equations. These equations are non-linear partial differential equations, that cannot be solved analytically, unless simple cases are studied that involve laminar flow and simple geometry, otherwise a numerical approach is mandatory. In particular, flow fluctuations due to turbulences are difficult to analyse and to study, even resorting to numerical simulations, and they are usually modelled using different methods to solve the Navier-Stokes equations. Since they are very expensive computational operations, different approaches have been developed based on the complexity of the case:

- **Reynolds Averaged Navier-Stokes (RANS):** these are Navier-Stokes equations where the quantities are averaged in a certain time interval, small enough with respect to the phenomena, but large enough with respect to the turbulence time scale in the flow. In this way the time required for the simulations is greatly reduced being that this method is not able to simulate the fluctuation deriving from the turbulence.
- **Large Eddy Simulations (LES):** this method is a good compromise between RANS (less time consuming but less precise) and DNS (more precise but more time consuming) approach. Differently from the RANS models, this approach simulates the larger vortical structures and model the smaller turbulences, resulting in a more accurate solution than RANS equations.
- **Direct Numerical Simulation (DNS):** it is the most complete model, the Navier-Stokes equations are completely solved without modelling any scale of turbulence. For this reason it is very time demanding, and it is

unthinkable to use this approach for industrial application, where the complexity of the cases would require computing power greater than the most powerful computer available nowadays.

Apart from the three fundamental models to solve the Navier-Stokes equations, also other models can be implemented that are a compromise between RANS and LES approach, such as SAS (Scale Adaptive Simulation) and SBES (Stress-Blended Eddy Simulation) models. These hybrid models enable to have slightly better results than simple RANS models limiting the time required for the simulation.

In order to solve this numerical models, a discretization process is required. This process is a method to represent and evaluate partial differential equations as algebraic equations. An iterative procedure is required in order to obtain the best solution possible. Discretisation models used are:

- **Finite volume method:** the partial differential equations are integrated in a volume and the boundary conditions are imposed on the boundaries of such volumes. The approximation comes from the fact that these volumes have a finite dimension and are not infinitesimal. Dividing the entire computational domain in small volumes, integrating the equations, in such a way the relations between the small volumes are written and solved numerically with the software.
- **Finite element method (FEM):** this is the most used numerical approximation approach. This method is particularly good when the computational domain is very complex and might have irregularities and enables to solve parts of the domain more accurately if a specific zone of the domain is of interest. The approach is to discretize the domain in a grid, so called mesh, made of finite elements that can have different shapes. The solution of the problem comes from a combination of functions, known as shape functions, and since it is an approximation, the values of the function are not necessary the exact values, but the correct values are those that give the smallest error.

- **Finite Difference Method (FDM):** this is an alternative solution to approximate the solutions of differential equations into partial differential equations. The main differences with the FEM approach are:
  - Finite elements allow for a better control of complex geometries with more ease. Finite differences are more restricted to simpler geometries.
  - Finite elements are easier to implement.
  - The approximation of finite elements has a better quality than the finite difference approach.

### 3.2 Two equations turbulence models

The models based on the solution of Navier-Stokes equations require other equations to be solved. These are the equations of the turbulence models. They can be one-equation like the Spalart-Allmaras (S-A), two-equation like the k- $\omega$  and k- $\epsilon$ , and six-equations like the Reynolds stress equation model. The two-equation turbulence models used in this thesis are:

- **Standard k- $\omega$  (k-omega):** this model attempts to predict turbulence by using two partial differential equations for k and  $\omega$ . k is the turbulent kinetic energy, while  $\omega$  represents the specific rate of dissipation of the turbulent kinetic energy. This model works better in the inner region of the domain, far from the wall since it can be easily integrated in the viscous sub-layer [7].

$$\frac{\delta(\rho k)}{\delta t} + \frac{\delta(\rho u_j k)}{\delta x_j} = \rho \tau_{ij} \frac{\delta u_i}{\delta x_j} - \beta^* \rho \omega k + \frac{\delta}{\delta x_j} \left[ \left( \mu + \sigma_k \frac{\rho k}{\omega} \right) \frac{\delta k}{\delta x_j} \right] \quad (8)$$

$$\frac{\delta(\rho \omega)}{\delta t} + \frac{\delta(\rho u_j \omega)}{\delta x_j} = \frac{\alpha \omega}{k} \tau_{ij} \frac{\delta u_i}{\delta x_j} - \beta \rho \omega^2 + \frac{\delta}{\delta x_j} \left[ \left( \mu + \sigma_\omega \frac{\rho k}{\omega} \right) \frac{\delta \omega}{\delta x_j} \right] + \frac{\rho \sigma_d}{\omega} \frac{\delta k}{\delta x_j} \frac{\delta \omega}{\delta x_j} \quad (9)$$

- **SST k- $\omega$  (Shear Stress Transport k-omega):** this model is widely used and combines the k- $\omega$  and the k- $\epsilon$  models, so that the k-omega model is

used to model the inner region and the k-epsilon model to model the near-wall region.

$$\frac{\delta(\rho k)}{\delta t} + \frac{\delta(\rho u_j k)}{\delta x_j} = \tau_{ij} \frac{\delta u_i}{\delta x_j} - \beta^* \rho \omega k + \frac{\delta}{\delta x_j} \left[ (\mu + \sigma_k \mu_t) \frac{\delta k}{\delta x_j} \right] \quad (10)$$

$$\frac{\delta(\rho \omega)}{\delta t} + \frac{\delta(\rho u_j \omega)}{\delta x_j} = \frac{\gamma}{v_t} \tau_{ij} \frac{\delta u_i}{\delta x_j} - \beta \rho \omega^2 + \frac{\delta}{\delta x_j} \left[ (\mu + \sigma_\omega \mu_t) \frac{\delta \omega}{\delta x_j} \right] + 2(1 - F_1) \frac{\rho \sigma_{\omega 2}}{\omega} \frac{\delta k}{\delta x_j} \frac{\delta \omega}{\delta x_j} \quad (11)$$

- **Standard k-ε (k-epsilon):** as for the k-ω model, the k-ε tends to predict turbulence by means of the k equation and the ε equation, representing the rate of dissipation of turbulent kinetic energy. This model works better in the shear region rather than in the inner region as for the k-omega turbulence model.

$$\frac{\delta(\rho k)}{\delta t} + \frac{\delta(\rho u_i k)}{\delta x_i} = \frac{\delta}{\delta x_j} \left[ \frac{\mu_t}{\sigma_k} \frac{\delta k}{\delta x_j} \right] + 2\mu_t E_{ij} E_{ij} - \rho \epsilon \quad (12)$$

$$\frac{\delta(\rho \epsilon)}{\delta t} + \frac{\delta(\rho u_i \epsilon)}{\delta x_i} = \frac{\delta}{\delta x_j} \left[ \frac{\mu_t}{\sigma_\epsilon} \frac{\delta \epsilon}{\delta x_j} \right] + C_{1\epsilon} \frac{\epsilon}{k} 2\mu_t E_{ij} E_{ij} - C_{2\epsilon} \rho \frac{\epsilon^2}{k} \quad (13)$$

### 3.3 CFD procedure

The typical approach requires to discretise the domain in cells creating a mesh on which apply the iterative method of resolution to solve the Navier-Stokes equations. The procedure to follow in order to solve the CFD problem is the same regardless the method used to solve the equations and the method used to discretize the computational domain.

1. Pre-processing: the geometry is defined according to what is the problem to analyse.
2. The volume of the computational domain is discretized and the mesh is generated.

3. The physical model is defined (equation of motion, equation of energy, ...) as well as the numerical model (discretization method of the equations, algorithm for the resolution of the equations).
4. Definition of the boundary conditions. The properties of the fluid are defined in the domain.
5. The simulation can start. The equations are solved iteratively and the computation is stopped when the results of the solution converge.
6. Post-processing: the results are visualised by means of appropriate tools, or by the CFD software itself.

Extensive CFD simulations have been performed, investigating both film cooling effectiveness and discharge coefficient, as well as fillet radius effects. The main object was to investigate aerothermal-fluid-dynamic of film cooling at different flow and geometrical properties. This investigation had also the goal to analyse the solutions not only from a mere academic and theoretical point of view, but also thinking from an industrial point of view where the simulations must have a compromise between time demand and accuracy of the results and the same results must be reached with as less effort as possible.

The thought process behind this work started from having a general idea of what results were likely to be achieved. The idea was to investigate the film cooling performance at different level of blowing ratio (0.5 – 1.0 – 1.5) solving the simulations with different two-equation turbulence models (standard  $k-\omega$ , SST  $k-\omega$  and standard  $k-\epsilon$ ) for a simple steady RANS approach. Fillet radius investigation was added at the end of the previous study, always analysing the film cooling performance, comparing the experimental results by means of film cooling laterally averaged effectiveness and discharge coefficient.

Everything started from the creation of the computational domain. The experimental case studied from the TATEF [\[1-2\]](#) has been taken into consideration to have a direct comparison of the results later on during the post-processing, hence the geometry has been modelled to achieve the

same flow and geometrical parameters used with the experimental set up. Once the geometry has been defined, the grid has been generated. Two cell elements have been used: tetrahedral and polyhedral cell volumes with different number of elements for each of these grids. As presented later on, in the case of polyhedral mesh, the total number of cells in the entire domain is approximately one third of the corresponding tetrahedral mesh, hence, for this reason, only three levels of polyhedral mesh have been generated. Converting 800 thousand elements in polyhedrons would have resulted in very few elements. Generating four different levels of the mesh has been necessary to do a grid sensitivity analysis to obtain results as much accurate as possible and, at the same time, to not use a mesh too much fine when the independency of the parameters was achieved with less elements and so the computational time would have been greater. In order to understand what was the most suited mesh, simulations with  $k-\omega$  turbulence model were run. Other two turbulence models, as well as other flow and geometrical features, were used once the mesh have been identified. Last simulations were run at different blowing ratios for all the three turbulence models.

In the last part of the study, the fillet radius effect has been investigated, from the sharp edge condition, as for the experimental setup, up to a radius value equal to 15% the diameter of the channel. This investigation has been done with SST  $k-\omega$  turbulence model and using the chosen mesh from the previous analyses.

In the post-processing software the results are obtained, analysed, and compared.

Following, the test matrix definition is presented in Table [2](#), reporting all the simulations done in chronological order.

<b>Geometry creation</b>	
No filleted channel edges	
<b>Mesh sensitivity analysis with k-<math>\omega</math> and BR = 1.0</b>	
Tetrahedral:	Polyhedral:
<i>Coarse mesh</i> [800k elements]	–
<i>Intermediate mesh</i> [1.6M elements]	<i>Intermediate mesh</i> [640k elements]
<i>Fine mesh</i> [3M elements]	<i>Fine mesh</i> [1.2M elements]
<i>Ultrafine mesh</i> [6M elements]	<i>Ultrafine mesh</i> [2M elements]
<b>Effect of the production limiter</b>	
<b>SST k-<math>\omega</math> and k-<math>\epsilon</math> applied to the selected mesh at BR = 1.0</b>	
Channel sharp edges	Channel filleted edges 5% D
<b>SST k-<math>\omega</math> and k-<math>\epsilon</math> at BR = 0.5 and BR = 1.5</b>	
Channel sharp edges	Channel filleted edges 5% D
<b>Effect of fillet radius at three levels of BR with SST k-<math>\omega</math></b>	

*Table 2 Test matrix definition*

## 4 Test case description and pre-processing

The test case studied refers to the experimental investigation carried out at the Institut für Thermische Strömungsmaschinen in Karlsruhe, Germany, in the Turbine Aero-Thermal External Flows (TATEF) project. The goals of this project are to have an insight on the aero-thermal phenomena generated in turbines, information necessary to improve turbine performance and life. The project investigated several phenomena of both flow and geometrical nature, such as discharge coefficient, lateral interaction of film cooling holes, turbulence intensity effects, film cooling rows interaction, and wake passing effects on film cooling. For the purpose of this work only data related to discharge coefficient and lateral interaction are considered.

The computational domain has the same geometrical features of the experimental setup. The channel has a cylindrical shape with injection angle  $\alpha = 30^\circ$  with respect to the hot gas stream. The hole diameter is  $D = 5\text{mm}$  and the length of the channel is  $L = 6D$ . The dimensions of the numerical domain are  $16D$  upstream the hole outlet and  $31D$  downstream the hole outlet. The width of the mainstream region is  $4D$ .

Figure [14](#) shows the domain representing the experimental setup in the best way possible to obtain the same flow and geometrical conditions. The experimental test case does not have a fillet in correspondence of neither the inlet nor outlet sections of the channel, thus the computational domain has been built up with sharp edges. The first simulations are run using this specific geometric setup, but during this study other computational domains have been created with different geometrical features. Different dimensions of fillet radius have been introduced at the junction of the cooling channel with both the plenum wall and the mainstream cooled surface. The introduction of the fillet has been done originally to create a better mesh with an appropriate orthogonality of the elements and also because in reality such thing as a sharp edge does not exist, there are always some machining errors during manufacturing operations independently on how accurate the

machine is. The fillet radius was set equal to 5% of the diameter of the hole, according to [8].

Other than a fillet radius of  $0.05D$ , different dimensions of the radius have been used to understand the impact of the fillet radius on the film cooling performance. The radii are equal to: 1.25%, 2.5%, 3.75%, 7.5%, 10% and 15% of the channel diameter.

The pre-processing procedure to create the geometries has been developed in ANSYS Design Modeler.

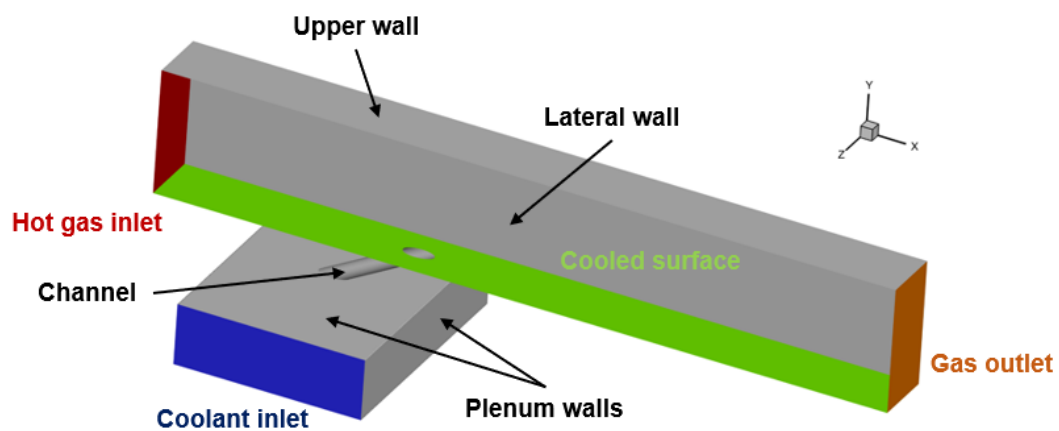


Figure 14 Computational domain

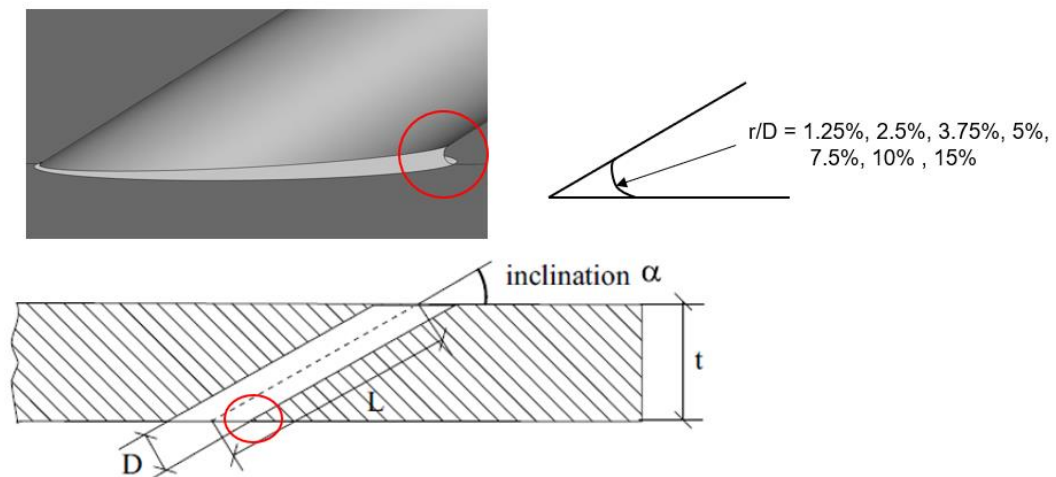


Figure 15 Fillet geometry

## 5 mesh sensitivity analysis

For the current investigation two types of hybrid mesh were used, a tetrahedral mesh and a polyhedral mesh, both with prismatic elements close to the walls. The meshes were generated using ANSYS Meshing.

Adiabatic and no-slip conditions were applied to the surfaces and the numerical campaign has been carried out on half the computational domain, since symmetric, hence a symmetry condition has been applied on the surface, and a periodic boundary condition on the lateral wall to simulate for a hole spacing of four diameters as for the experimental setup.

A sensitivity analysis was performed on both grids at blowing ratio condition  $BR = 1$ . For both tetrahedral and polyhedral mesh the approach for the construction of the mesh has been the same. Since the region of interest of this investigation is the downstream region of the outlet hole, the mesh has been refined in proximity of that region, increasing the number of elements in that volume zone and on the cooled surface downstream the hole. An inflation layer with twenty-one prismatic layers have been created above the cooled region to have a better boundary layer modelling.

Following, the number of elements of both meshes are reported in Table 3. Four grids have been generated for the tetrahedral mesh and three grids for the polyhedral. Polyhedral mesh has a smaller number of total elements compared to tetrahedral mesh, this is the reason why the denoted *Coarse mesh* has not been generated with polyhedral elements, otherwise the grid would have resulted with too few cells and the results would not have been accurate.

	<b>Tetrahedral mesh</b> <b>[millions of elements]</b>	<b>Polyhedral mesh</b> <b>[millions of elements]</b>
<b>Coarse mesh</b>	0.8	-
<b>Intermediate mesh</b>	1.6	0.64
<b>Fine mesh</b>	3	1.2
<b>Ultrafine mesh</b>	6	2

Table 3 Mesh parameters

The polyhedral mesh has been created in two ways: converting the tetrahedral into polyhedral cells, and the second method has been by generating the mesh from scratch, meaning no tetrahedral has been created to obtain the polyhedral elements. The difference between the two generation was not noticeable in the total number of elements, since it was basically the same, rather on the quality of the mesh. Creating the polyhedral from converting the elements of the tetrahedral resulted in a bad mesh quality with elements that were not polyhedrons (Figure 16 is an example of this problem in the channel region). For this reason the polyhedral mesh used was the grid generated without starting from the tetrahedral.

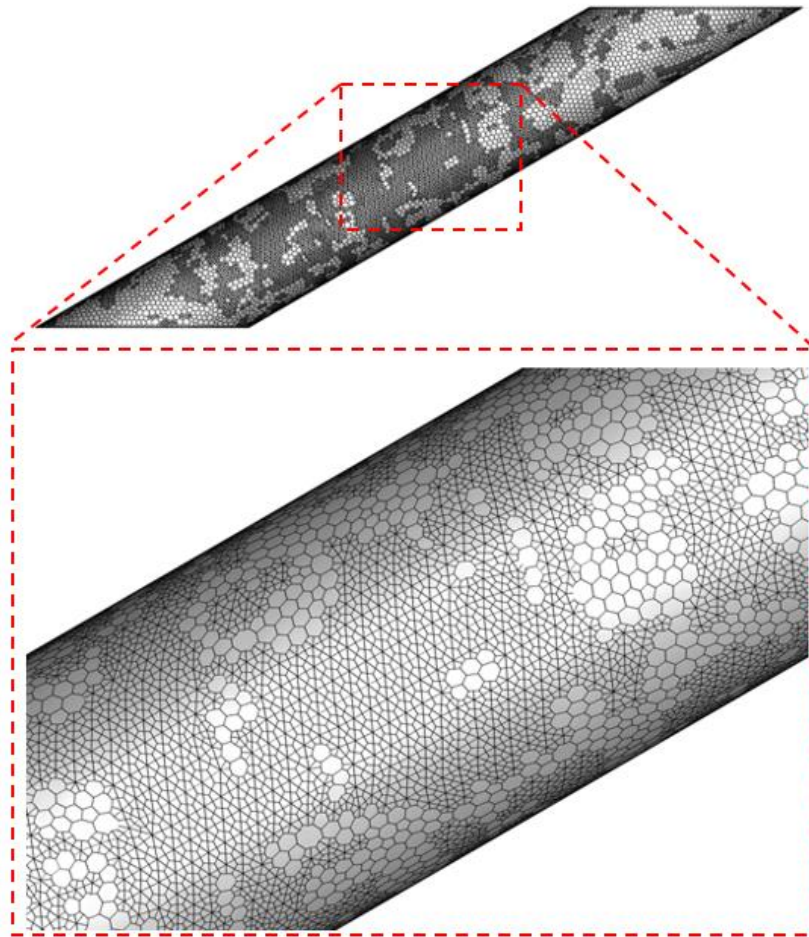


*Figure 16 Detail of polyhedral mesh from converted tetrahedral grid*

In order to select the appropriate number of elements and the correct element geometry, the results of adiabatic effectiveness as well as laterally

averaged effectiveness have been compared to see when the independently of the parameters on the mesh is reached.

First the solutions have been compared between results obtained with the same cell geometry for different elements size, and consequently the results have been compared between the two types of mesh.

Figure 17 shows local adiabatic effectiveness maps at different mesh sizes for the tetrahedral case, whereas Figure 18 shows the same maps for the polyhedral case.

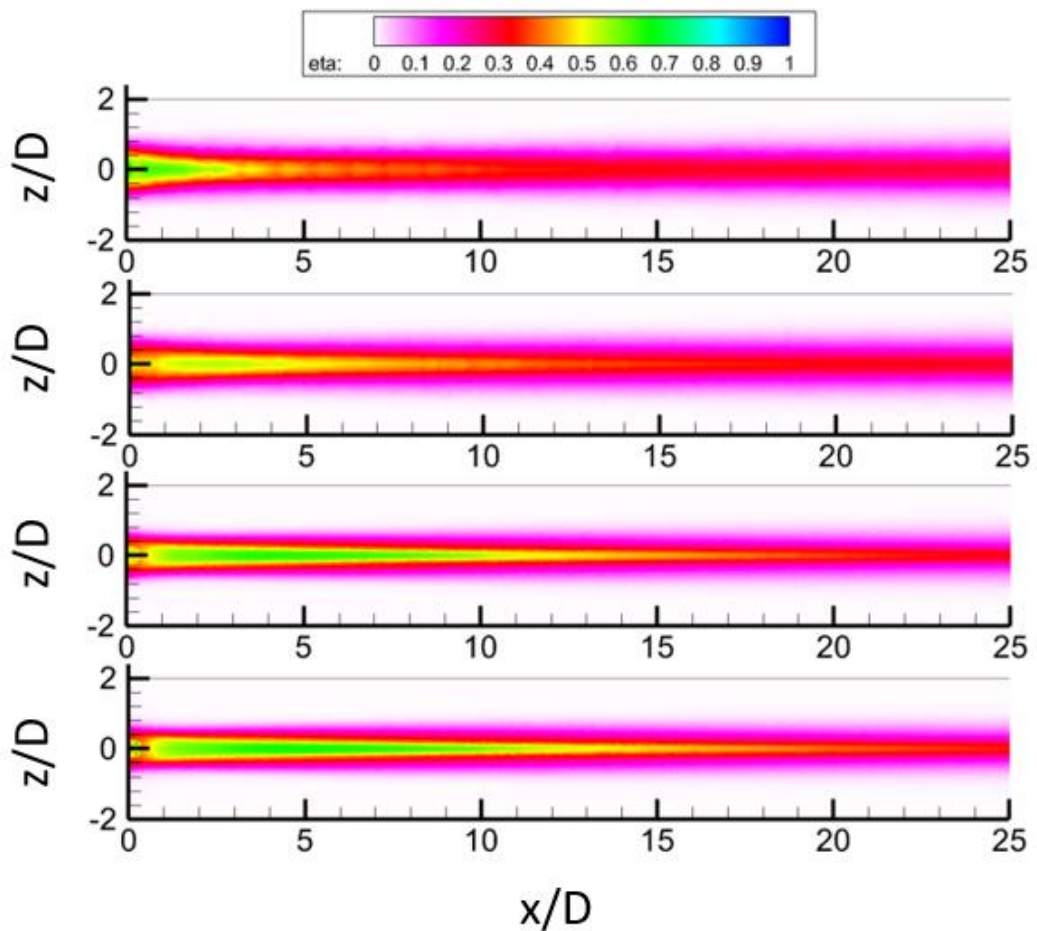


Figure 17 Local effectiveness  $BR=1.0$  Tetrahedral Coarse mesh (top), Intermediate mesh, Fine mesh, Ultrafine mesh (bottom)

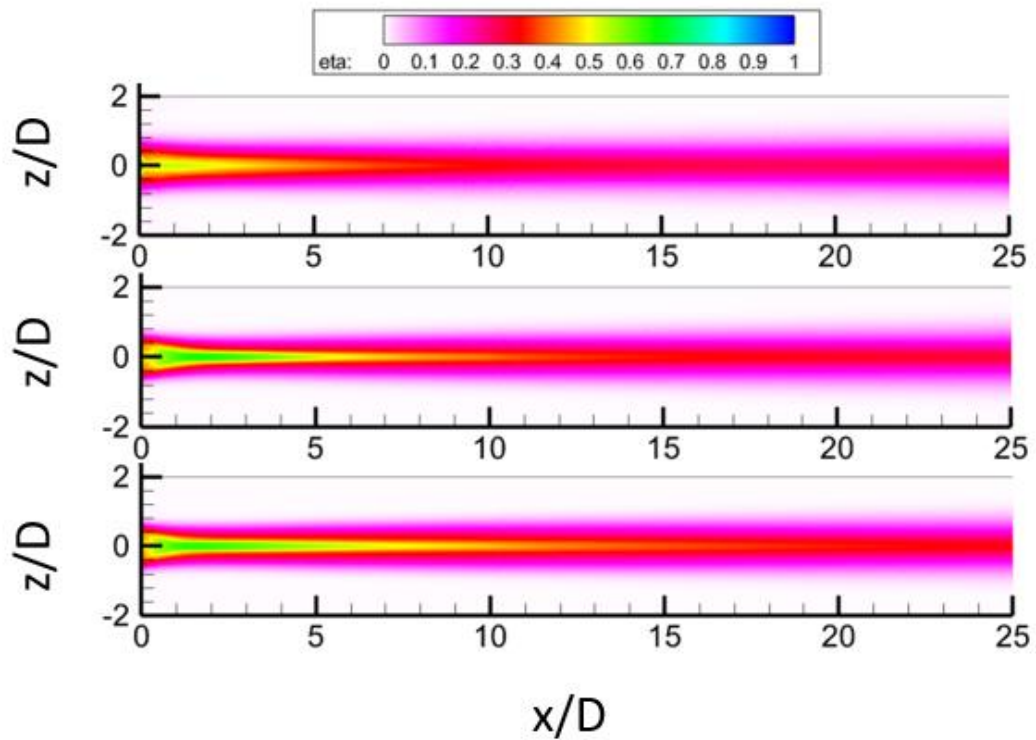


Figure 18 Local effectiveness  $BR=1.0$  Polyhedral Intermediate mesh (top), Fine mesh, Ultrafine mesh (bottom)

Comparing the results obtained, *fine* and *ultrafine* grids seem to give similar solutions for both the tetrahedral and polyhedral element. The choice of the mesh is not only based on effectiveness maps but also comparing the laterally averaged values of film cooling effectiveness to have a more direct comparison between the results, as shown in Figure [19](#).

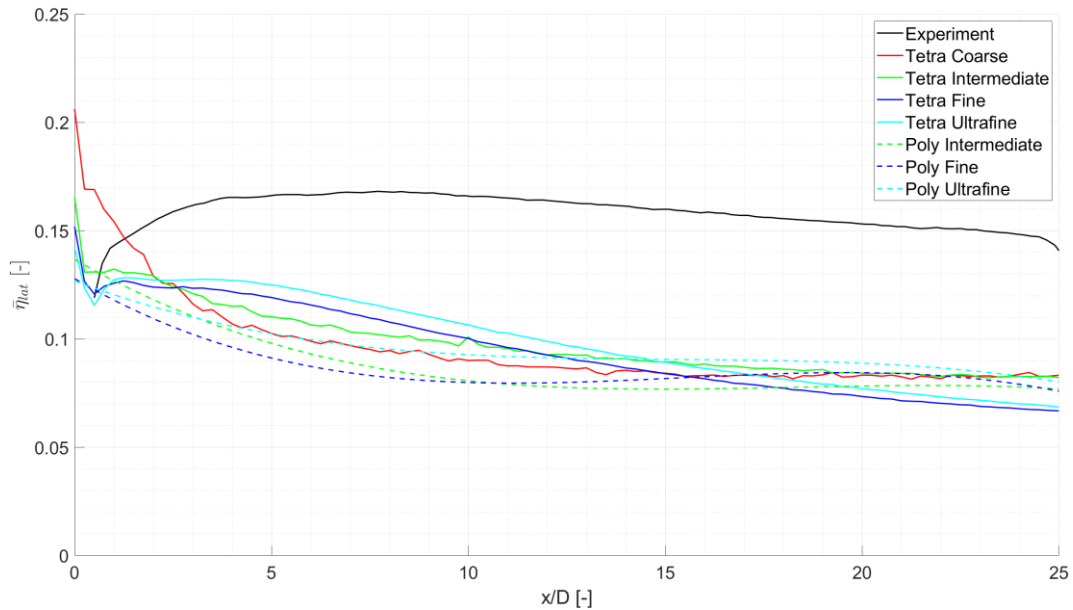


Figure 19 Laterally averaged effectiveness  $BR=1.0$  Comparison between tetrahedral and polyhedral mesh

As shown in the above figure, it is assessed that the *fine* and *ultrafine* results are very similar in particular for the tetrahedral mesh. The optimal case to carry out the study for this thesis seems to be the tetrahedral mesh *Fine mesh*, and it is going to be the mesh used throughout the rest of the work. However, to not jump to too hasty conclusions, a deeper investigation of the results obtained is mandatory also to better understand why there are these differences between the simulations. Hence, since the distribution of the coolant over the surface is strictly dependent on the development of the coolant inside the channel, an investigation of such phenomenon is done, analysing sections of the channel perpendicular to its axis by means of the Mach number. Moreover, the Mach number in the middle plane of the channel is plotted in order to have a wider vision of the coolant evolution inside the channel to see where the coolant detaches inside the hole. Based on the previous images the *Fine mesh* is the best suited for both the grids, tetrahedral and polyhedral, hence the investigation of the coolant in the channel is carried on for these grid. Figure [20](#) shows four channel sections equidistant to each other, and Figure [21](#) shows the differences along the entire length of the channel.

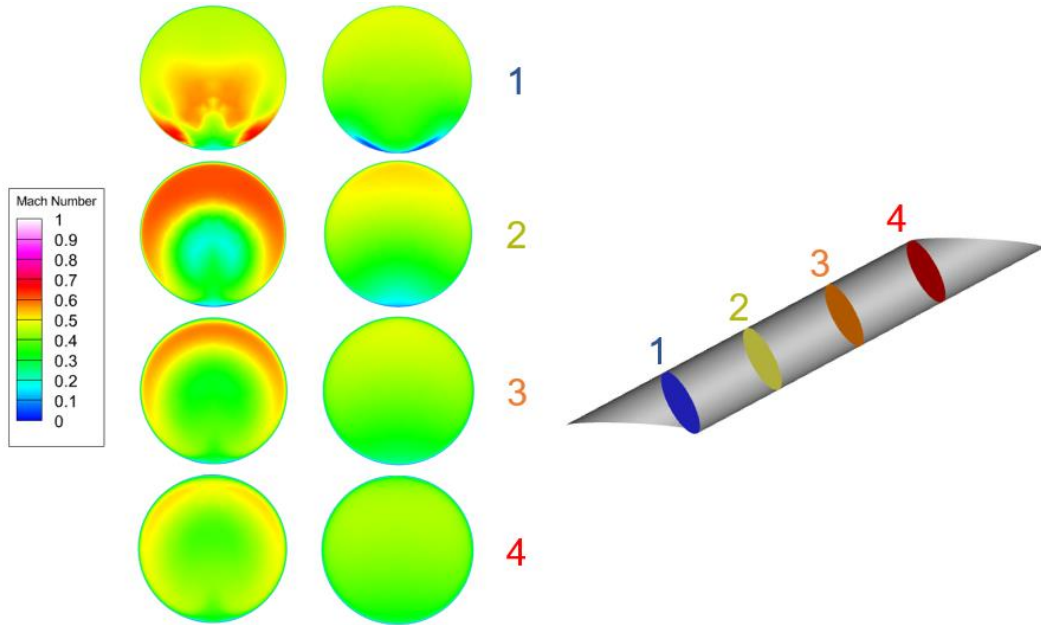


Figure 20 Mach number sections perpendicular to the channel axis: Tetrahedral (left) Polyhedral (right)

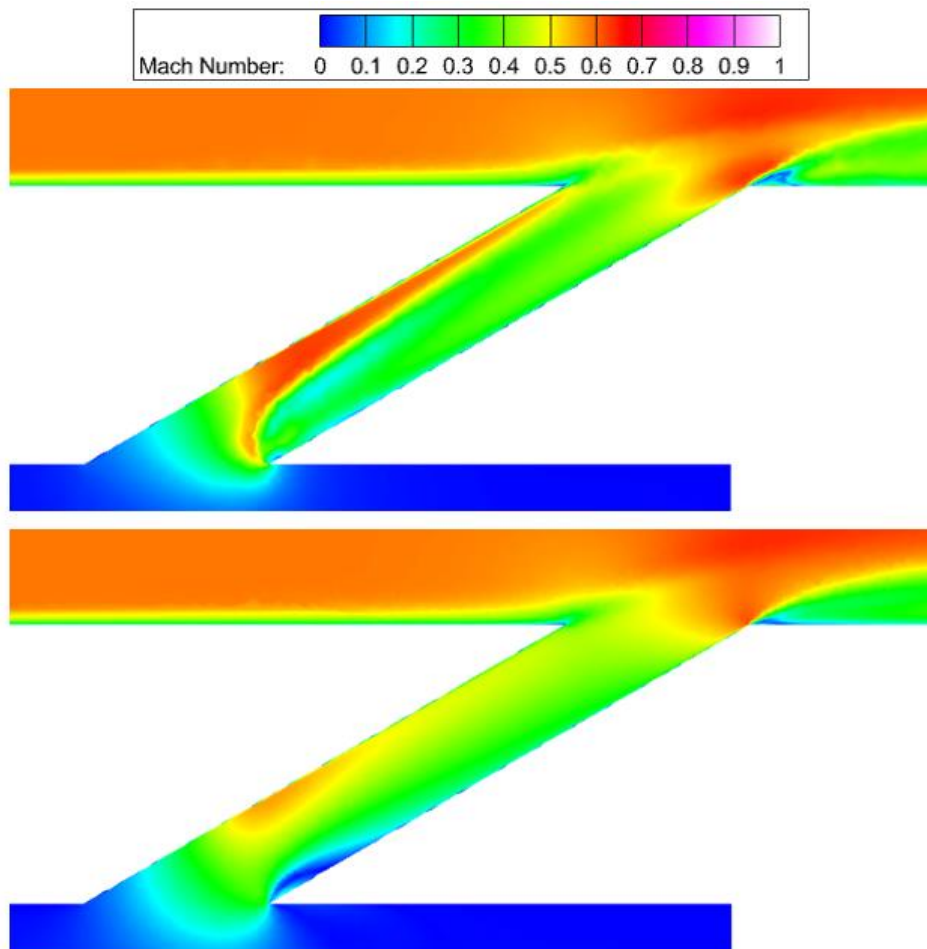


Figure 21 Symmetry plane Mach number in the channel: Tetrahedral (top) Polyhedral (bottom)

As for the local effectiveness, how the coolant develops in the channel is very different between the two cases. In the polyhedral mesh the coolant has a more uniform velocity throughout the entire length of the hole, whereas in the tetrahedral case the coolant has low velocity in the middle of the channel and a sort of ring at higher velocity is formed adjacent the wall channel. From this results it seems as if the coolant is able to completely develop in the polyhedral case mid-way the channel length, differently from the other mesh case. The difference is very noticeable even looking at the symmetry plane, where it is clear for the polyhedral case that almost the flow immediately reattaches at the wall as if the coolant enters with less velocity.

Velocity vectors on the symmetry plane are checked to understand why there are these vast differences between the two cases. Figure [22](#) shows that a completely unexpected phenomenon occurs in the polyhedral solution. Surprisingly, a recirculation is generated in correspondence of the inlet hole where the coolant has to do a tight curve to enter the channel. This vortex should not occur since in the plenum there is no coolant crossflow and the Mach number is null. Figure [23](#) shows the extension of such vortex and as can be seen, it spread all over the trailing edge part of the hole. On the contrary, it is shown that a uniform increase of velocity is obtained with the tetrahedral solution close to the inlet section.

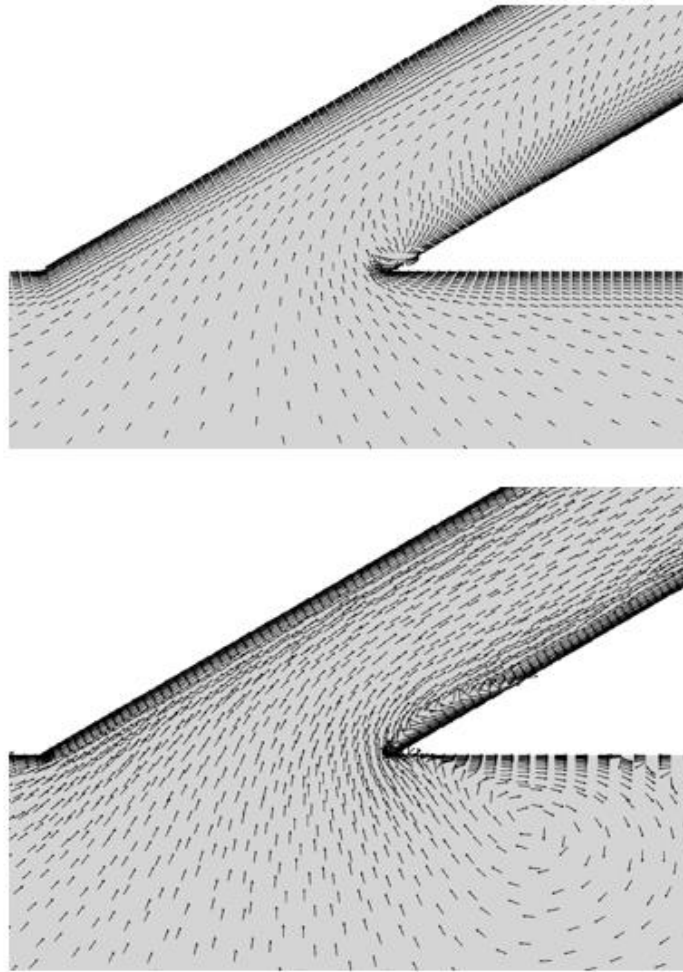


Figure 22 Symmetry plane velocity vectors: Tetrahedral (top) Polyhedral (bottom)

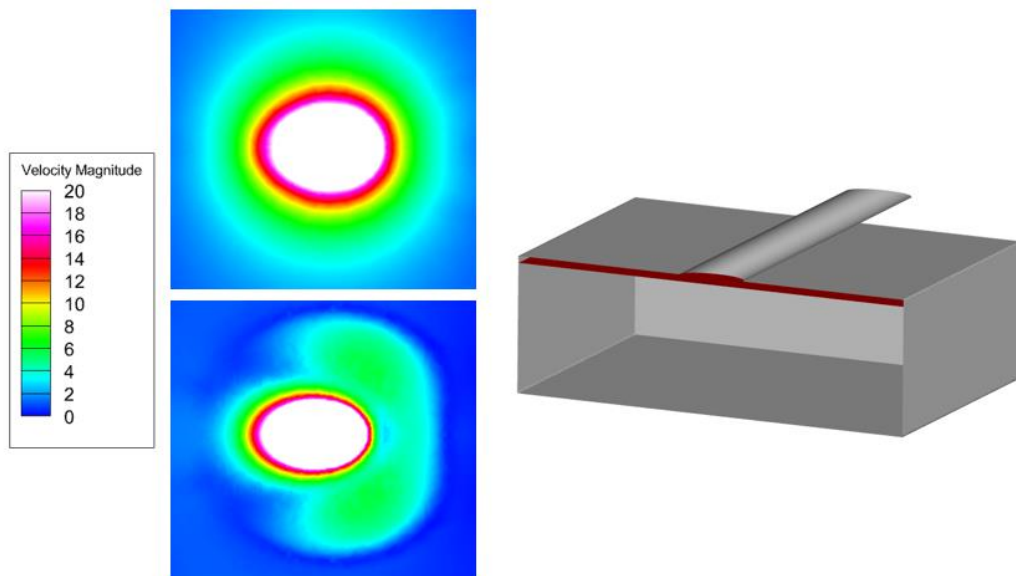


Figure 23 Velocity magnitude at the inlet hole. Extension of the recirculation for the polyhedral solution (bottom)

In order to try to solve this problem and obtain simulations that give approximately the same result, despite the mesh elements, a limiter has been introduced in the equations that solve the problem.

Two-equation turbulence models have a disadvantage, the excessive generation of turbulence energy close to the stagnation points. This excessive increase of turbulent kinetic energy can be seen at the entrance of the channel, where the turn the coolant has to do is quite important. For this reason, to avoid the buildup of turbulence energy, the production limiter term has been added. This solves the problem found with the polyhedral mesh.

Since the production limiter has been used for the polyhedral case, this parameter is added also to the tetrahedral grid to have a fair comparison between the results, even though the solutions are not influenced very much by the addition of this parameter. Following the figure with the new results are reported. Figure [24](#) shows, by means of the velocity vectors, that the recirculation previously found in the plenum is no more present and to further enhance this result obtained, Figure [25](#) show the comparison of Mach number along the channel. With the addition of the limiter the coolant development inside the channel is quite similar, compared to Figure [21](#) where they were completely different. Such similarity is better visualised in Figure [26](#) with section of the channel perpendicular to its axis.

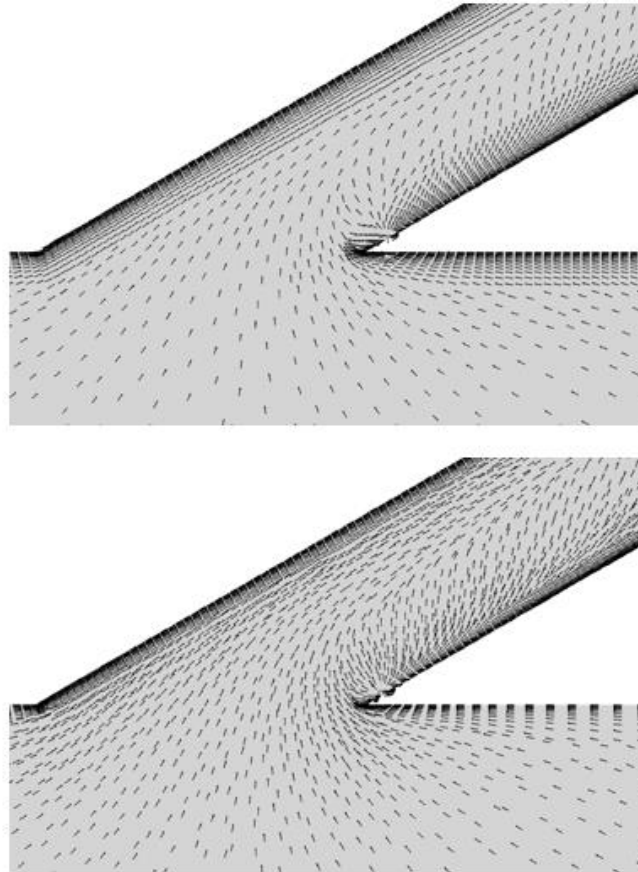


Figure 24 Symmetry plane velocity vectors: addition of the production limiter. Tetrahedral (top)  
Polyhedral (bottom)

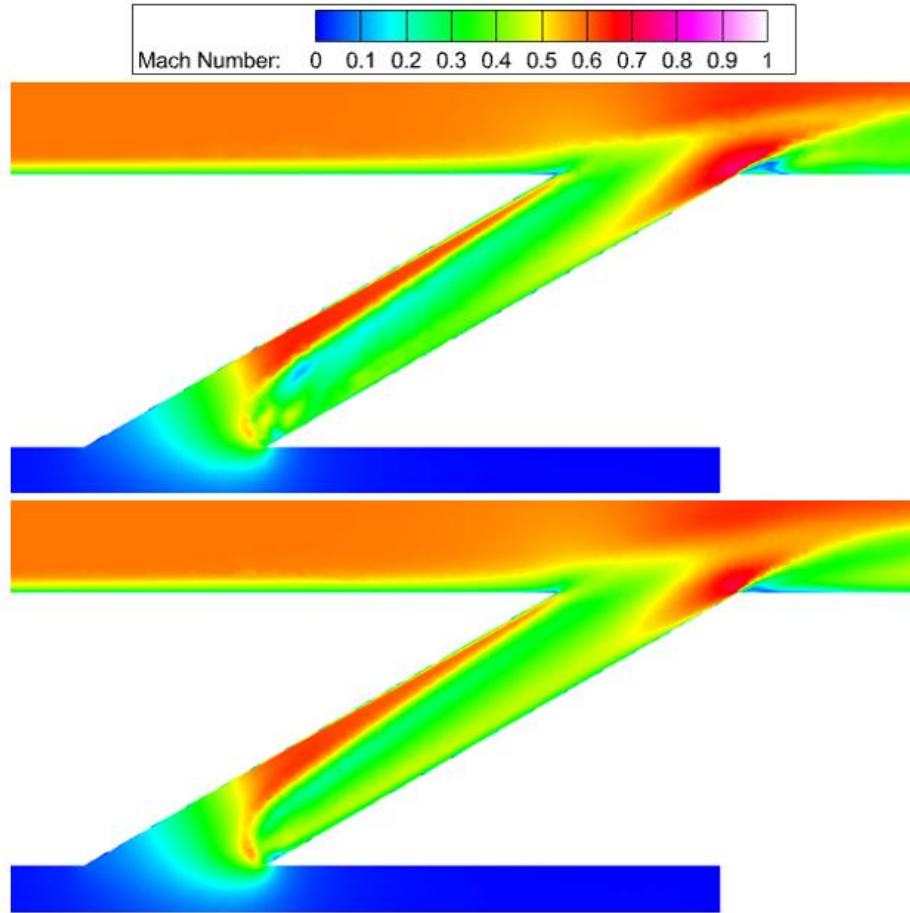


Figure 25 Mach number in the channel: addition of the production limiter. Tetrahedral (top)  
 Polyhedral (bottom)

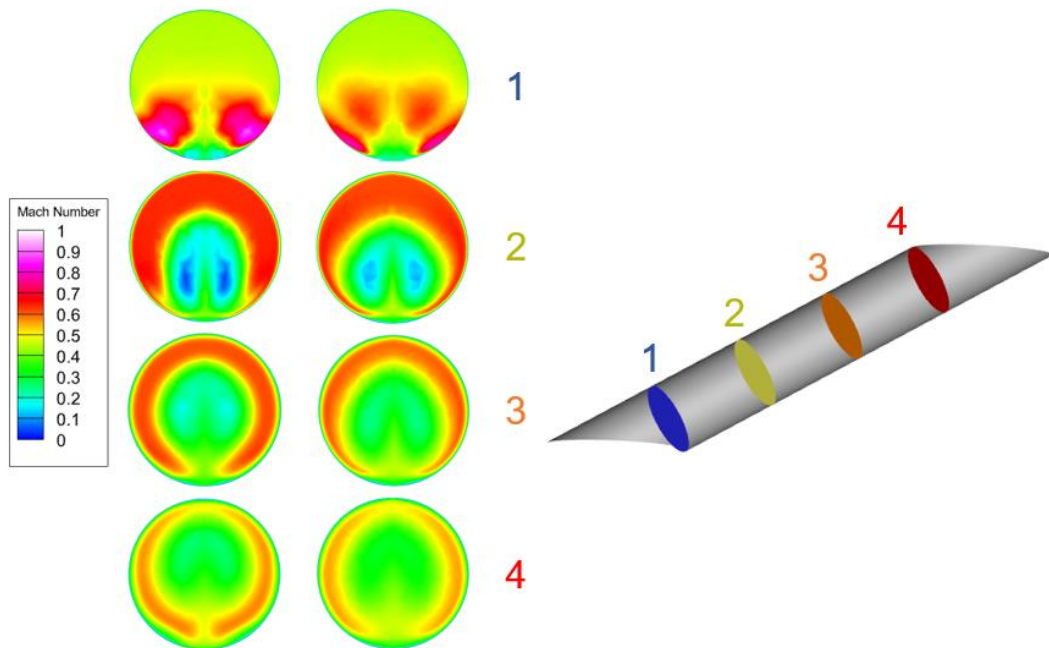


Figure 26 Mach channel sections perpendicular to the channel axis: addition of the production limiter. Tetrahedral (left) Polyhedral (right)

After analysing different cells geometry and different size meshes, some conclusions can be drawn on this first part of the work.

Mesh sensitivity analysis has been essential in order to assess what was the most suited grid to continue with. It came out after different comparisons that the tetrahedral *Fine mesh* resulted better than the rest of the grids. In this analysis a limiter has been necessary to use in order to obtain feasible results for the polyhedral mesh. In retrospect, the production limiter is a parameter that is always better to use, reason why the next simulations of this thesis will be all run with the production limiter activated.

Following, in Figure 27, the final results are reported, which in summary have been obtained at  $BR = 1.0$ , turbulence model  $k - \omega$ , production limiter on and tetrahedral mesh with three million elements.

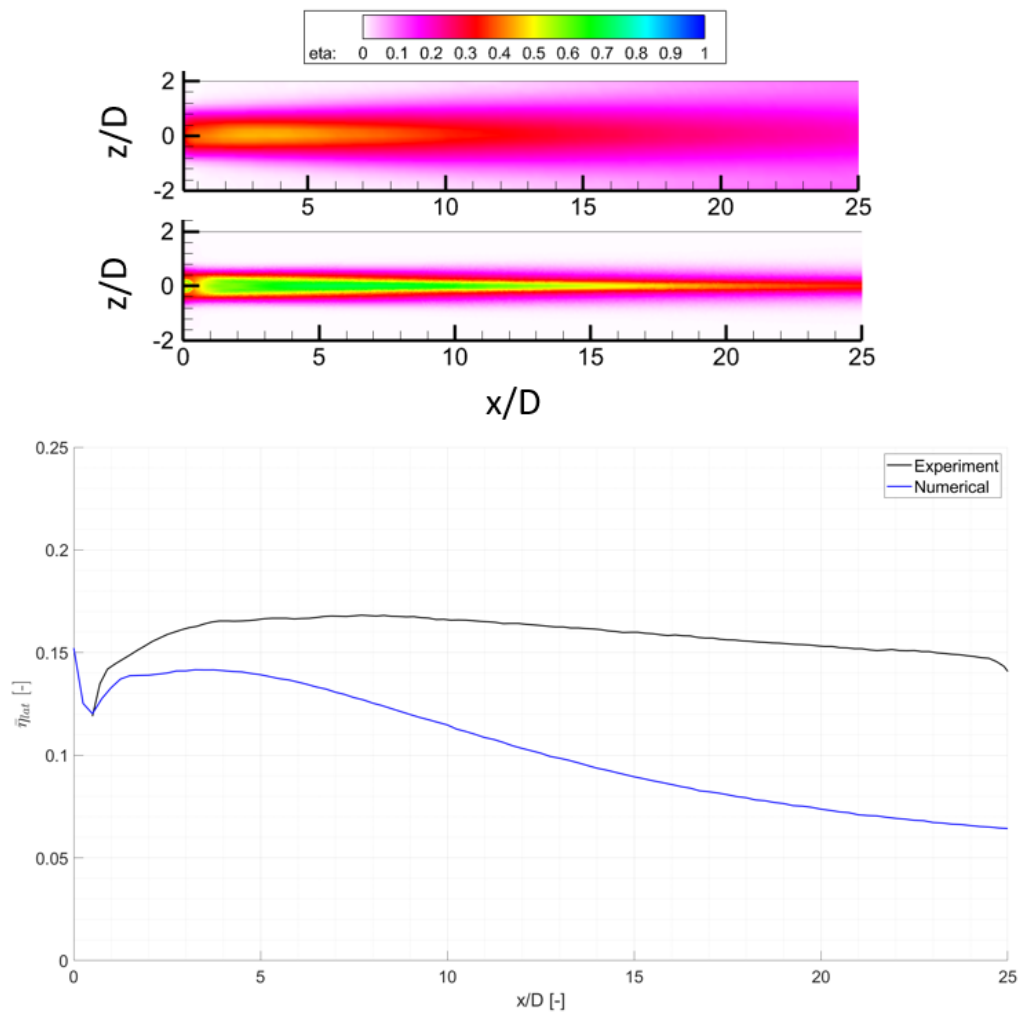


Figure 27 Local and laterally averaged effectiveness compared to experimental results

To conclude this chapter about the mesh generation and sensitivity study of the grid, figures (Figure 28-31) showing the tetrahedral mesh are presented to give an insight on how the mesh has been generated in the most critical points of the domain and in specific regions.

To notice that in Figure 31 is reported the close up of the mesh on the junction between the channel inlet and the plenum wall, reporting the mesh for different geometrical conditions of the fillet radius that will be studied later on in this work.

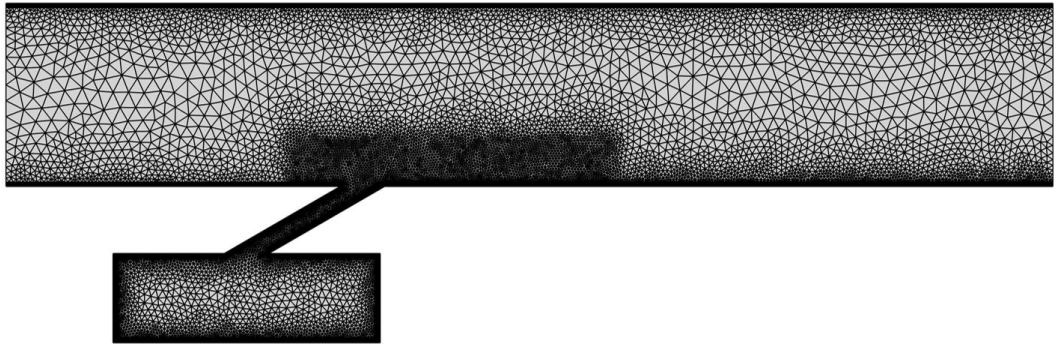


Figure 28 Computational domain mesh

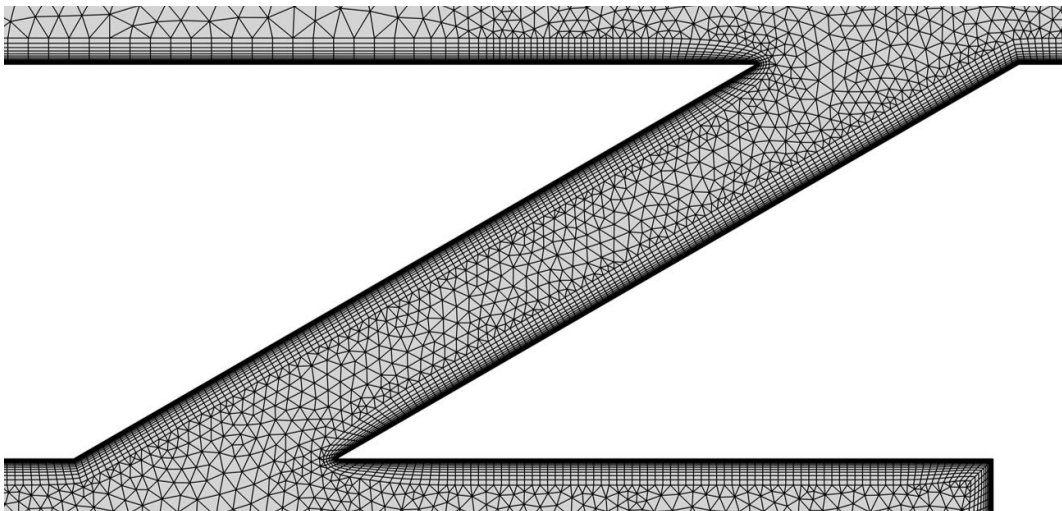


Figure 29 Channel mesh

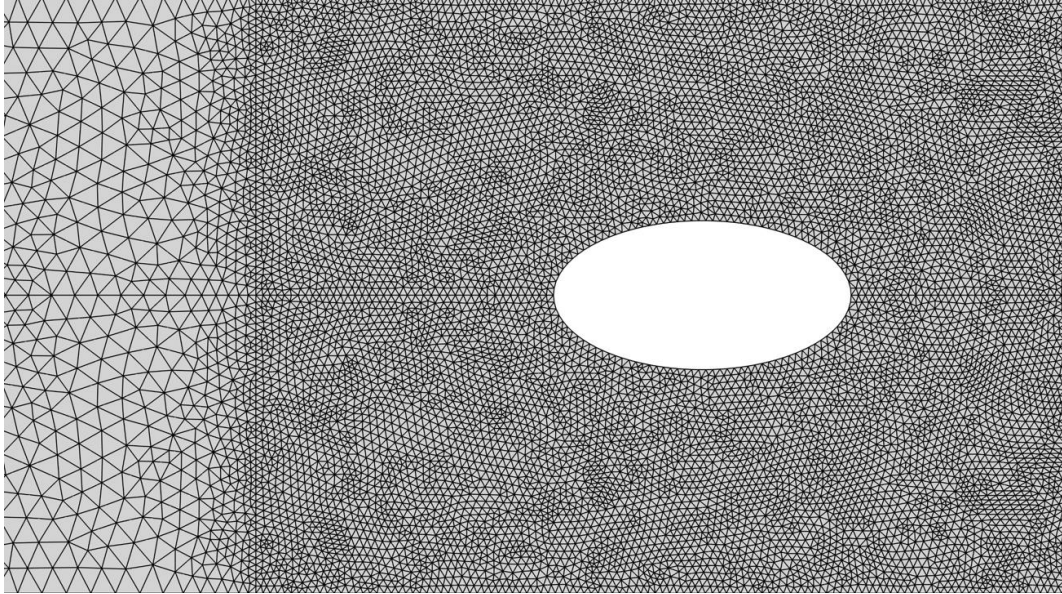


Figure 30 Cooled surface mesh

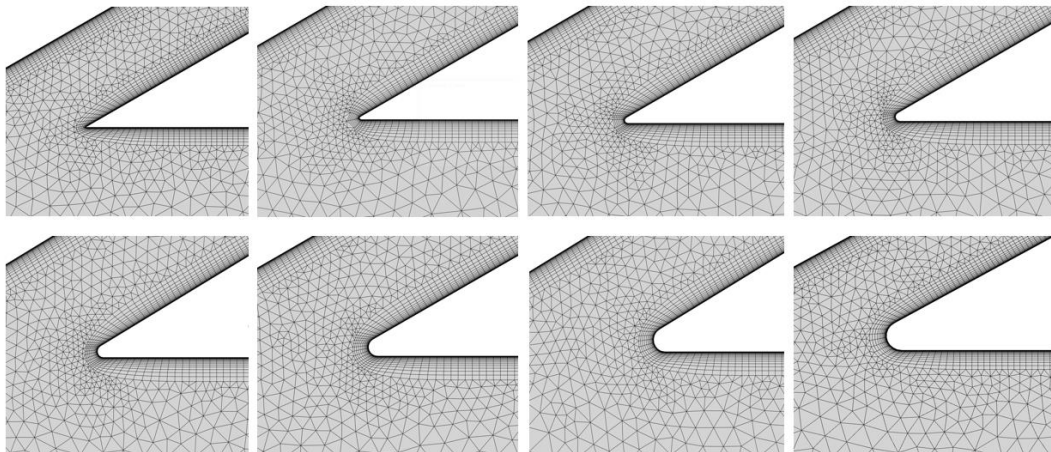


Figure 31 Fillet channel-plenum mesh: sharp edge, 1.25%D, 2.5%D, 3.75%D, 5%D, 7.5%D, 10%D, 15%D (from left to right, top to bottom)

## 6 Computational models and $\eta$ results

### 6.1 Boundary conditions

Numerical simulations were run in ANSYS Fluent. After the mesh has been generated, it has been imported in the software for the numerical analysis of the problem. Once imported the mesh and solved the discretization, it was time to select the regions and surfaces of the computational domain to apply the physical conditions of the problem, that is to say the boundary conditions of the problem. For this purpose on each surface of the domain a physical condition has been applied.

Following, the table (Table 4) resuming the boundary conditions applied is reported.

Hot gas total pressure [Pa]	126000
Coolant total pressure [Pa]	107500 – 126700 – 153400
Hot gas total temperature [K]	575
Coolant total temperature [K]	300
Hot gas Mach number [-]	0.6
Coolant Mach number [-]	0
Blowing ratio [-]	0.5 – 1.0 – 1.5

Table 4 Boundary conditions

Once the physical boundary conditions have been defined, the definition of the parameters to solve the problem is required, that is to say the models used by the algorithm to solve the problem. Three different turbulence models were used: *standard k- $\omega$* , *SST k- $\omega$*  and *standard k- $\epsilon$* .

### 6.2 Turbulence model comparison

With the sensitivity analysis of the mesh, the grid has been chosen to which apply the next simulations. The first part is devoted to the comparison of different turbulence models. Up until now the simulations used to analyse

the grid dependence were run using the k- $\omega$  turbulence model at unitary blowing ratio, while this part of the thesis is assessed to investigate which model is most suited to obtain results as close as possible to the experiment, with the aim to eventually choose the model that will be used in the next simulations, remembering that the goal of the work is not only a comparison between numerical and experimental results, but also to understand which are the best conditions to use to investigate on film cooling.

The comparison of the results is always done checking the local and laterally averaged effectiveness results. As done for the sensitivity analysis also velocity field and Mach number will be compared between models to have a stronger validation of the results.

The results compared until now use a computational domain with the sharp edge between the channel and the plenum and mainstream wall, but since in reality a proper sharp edge does not exist, it has been decided to add a fillet in correspondence of those edges equal to 5% the diameter of the channel, in this way the comparison have been done also with another geometrical setup that may give better results than the other case.

Before passing to the presentation and analysis of the results a consideration has to be done regarding the application of the turbulence models. Each pair of equations solves the problem in different ways as said at the beginning of this thesis (k- $\omega$  solves better the inner region, k- $\epsilon$  close to the walls, and SST k- $\omega$  is a mix between the two) and they require particular conditions for them to work properly. One such requirement is the  $y^+$  (yplus) parameter to be in certain range of values according to the model used. Low-Re models, such as k- $\omega$ , requires  $y^+ \leq 1$  leading to the requirement of abundant mesh cells close to the wall. On the other hand, the k- $\epsilon$  model requires  $30 < y^+ < 300$ , if the value is too low the model is not valid and the solution will not run. The mesh used has a  $y^+$  value smaller than one, hence in order to run the simulations using the k- $\epsilon$  model, it is required the creation of a new mesh, unless a good wall function is implemented. This is what has been done, a wall function called Enhanced Wall Treatment (EWT) has been added to the k- $\epsilon$  model. This enables the

model to run without having to change the mesh. This wall function is based on the combination of a blended law-of-the-wall, allowing for the incorporation of pressure gradient effects and thermal effects, and a two-layer zonal model used to determine near-wall  $\epsilon$  field.

Now that all the premises have been done, the results are now compared and discussed.

The easiest way is to compare the  $\bar{\eta}_{lat}$ , Figure 32, to immediately understand how the simulations compare to each other. It is clear that the geometry with the fillet radius gives a better prediction of the experimental data, especially when it comes to *SST k- $\omega$*  and *k- $\epsilon$*  turbulence model. All the models underestimate the experimental curve for all the downstream length except in correspondence of the region immediately downstream the hole, where an overestimation of the data is foreseen. Figure 33 represents the maps of  $\eta_{aw}$  corresponding to the curves of laterally averaged effectiveness plotted in Figure 32. As anticipated by looking at the curves, the filleted geometry gives better results, in particular it shows higher longitudinal coverage of the coolant compared to their respective sharp edge solutions.

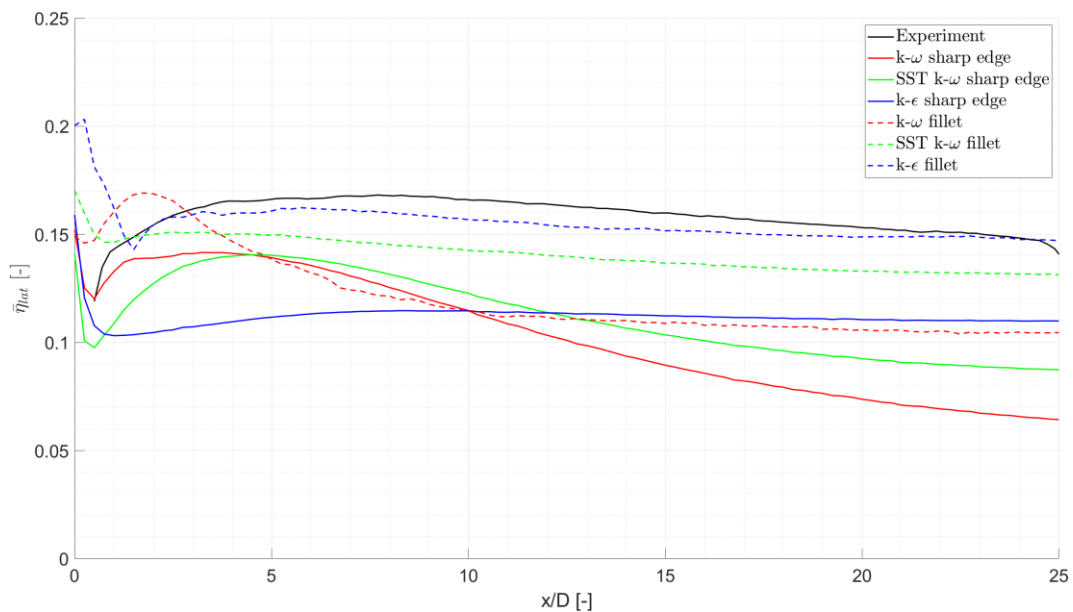


Figure 32 Comparison of  $\bar{\eta}_{lat}$  at different turbulence model and geometrical channel edges

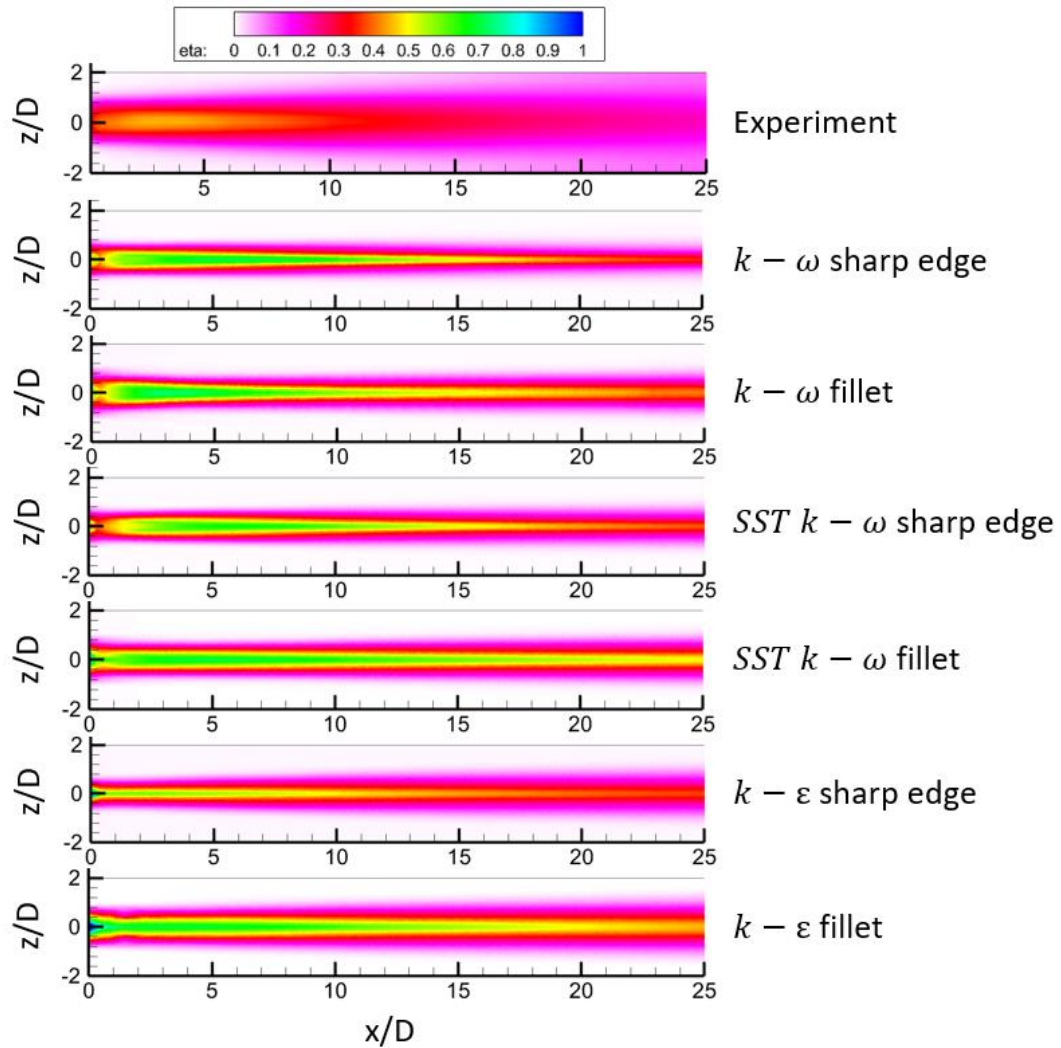


Figure 33 Corresponding  $\eta_{aw}$  of Figure 32

Figure 34 presents the Mach number inside the channel by means of sections perpendicular to its axis (see Figure 20 and 26 to see where the sections are located inside the channel). From this section it is evident why the effectiveness results differ from sharp edge and fillet condition. The addition of the fillet helps the coolant to enter the channel, reducing the losses and changing completely the development of the coolant throughout the hole. Low velocity region is confined closer to the wall of the channel for the filleted solution, hence the high velocity region has more space and consequently its velocity is also smaller than the corresponding sharp edge case. Having a low velocity region in the middle of the hole, as for the sharp edge solution, acts as a nozzle, reducing the space where the coolant can flow, hence, to pass a certain quantity of coolant its velocity needs to

increase, whereas with the filleted edge the low velocity region is smaller and the coolant has more space to pass, hence the velocity is slightly lower. This changes in development of the coolant bring to the differences seen in the effectiveness results.

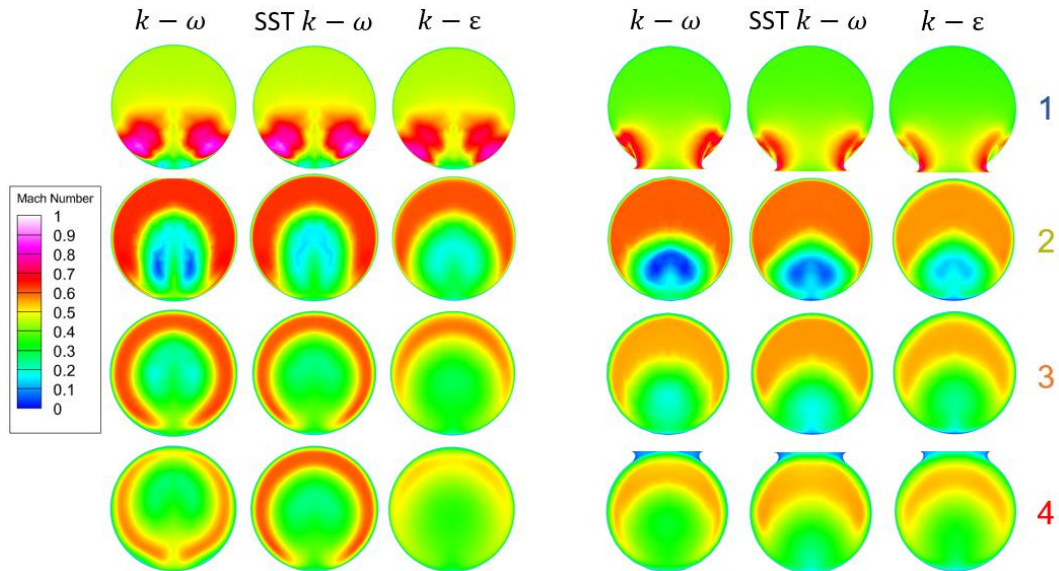


Figure 34 Mach number inside the channel. Sharp edge solutions (left) and filleted solutions (right)

Figures [35](#), [36](#) and [37](#) give a general overview of the development of the coolant inside the channel, showing the Mach number on the middle plane of the channel, proving what has been said by looking at the channel sections.

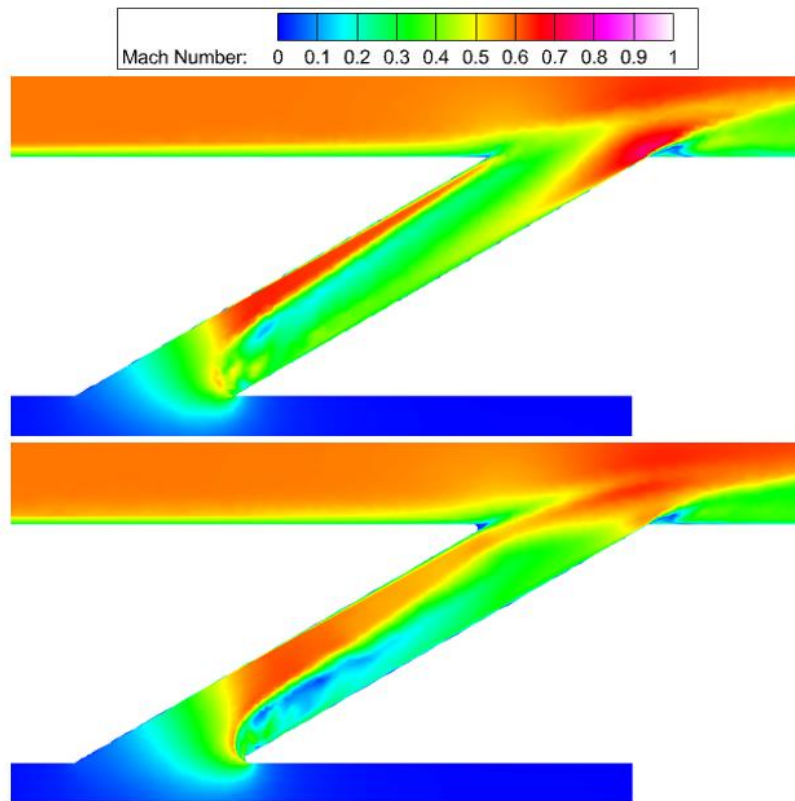


Figure 35 Mach number  $k-\omega$ , sharp edge (top) and fillet (bottom)

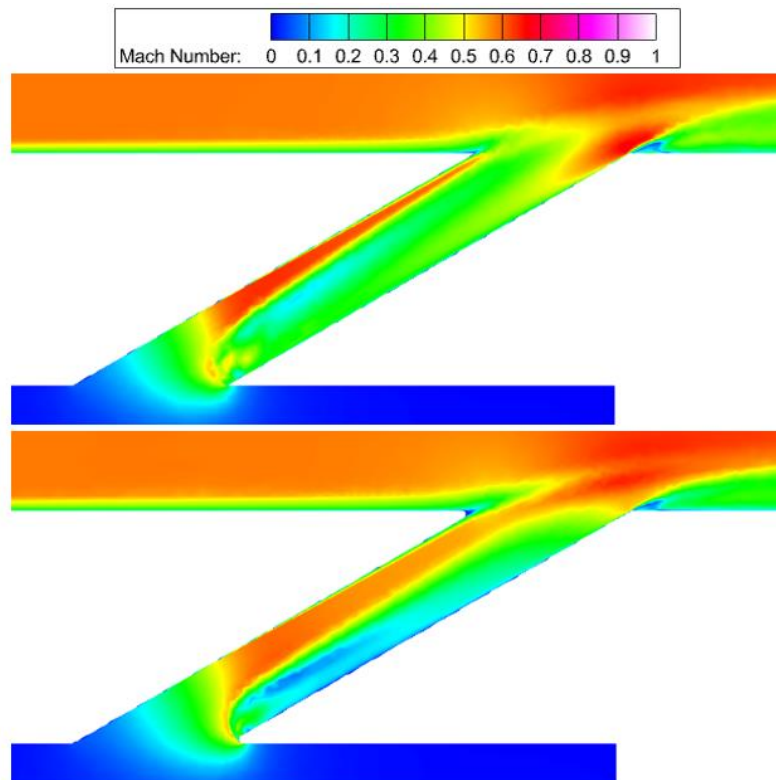


Figure 36 Mach number SST  $k-\omega$ , sharp edge (top) and fillet (bottom)

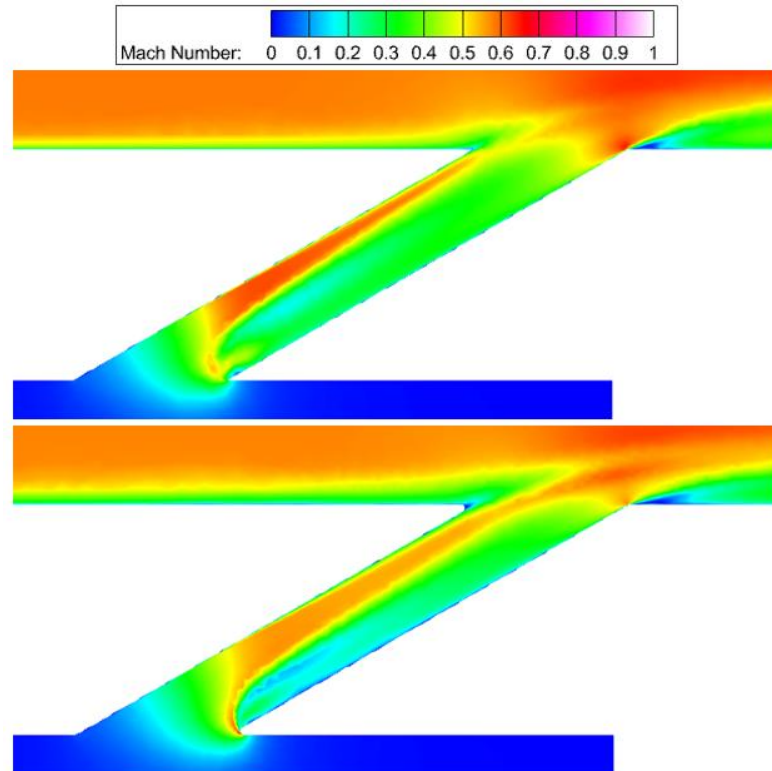


Figure 37 Mach number  $k-\epsilon$ , sharp edge (top) and fillet (bottom)

### 6.3 Blowing ratio effect

Different turbulence models have been tested and compared for two different geometrical conditions at the same blowing ratio value of  $BR = 1.0$ . From this comparison it came out that filleted edges can result in great improvement of the results. Based on the conclusions drawn and on the results obtained, the next simulations to compare the results at different blowing ratio conditions will be run using only  $SST k - \omega$  and  $k - \epsilon$  applied to the geometry with the fillet radius.

First of all, laterally averaged effectiveness curves are compared in Figure [38](#), showing the curve for both  $SST k - \omega$  and  $k - \epsilon$  at three levels of blowing ratio.

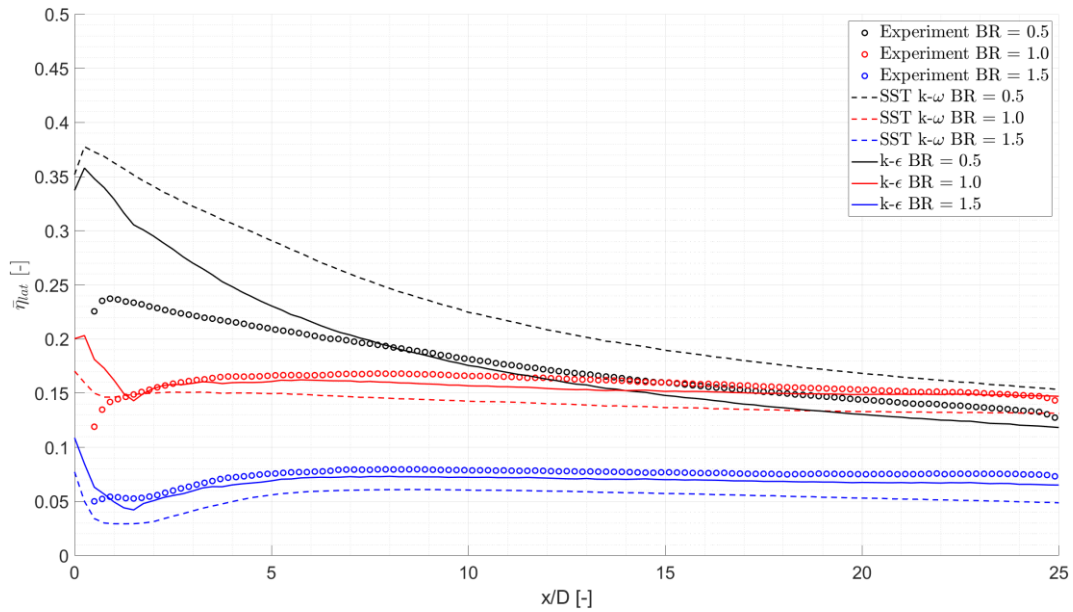


Figure 38  $\bar{\eta}_{lat}$  at  $BR=0.5$ ,  $BR=1.0$  and  $BR=1.5$

Results are very similar between the two turbulence models compared, only at  $BR = 0.5$  the difference is more significant, because as can be seen from the local adiabatic effectiveness map (Figure 39), at  $BR = 0.5$  the  $SST k - \omega$  model predicts a longer longitudinal coverage of the coolant on the surface with respect to the  $k - \epsilon$  model.

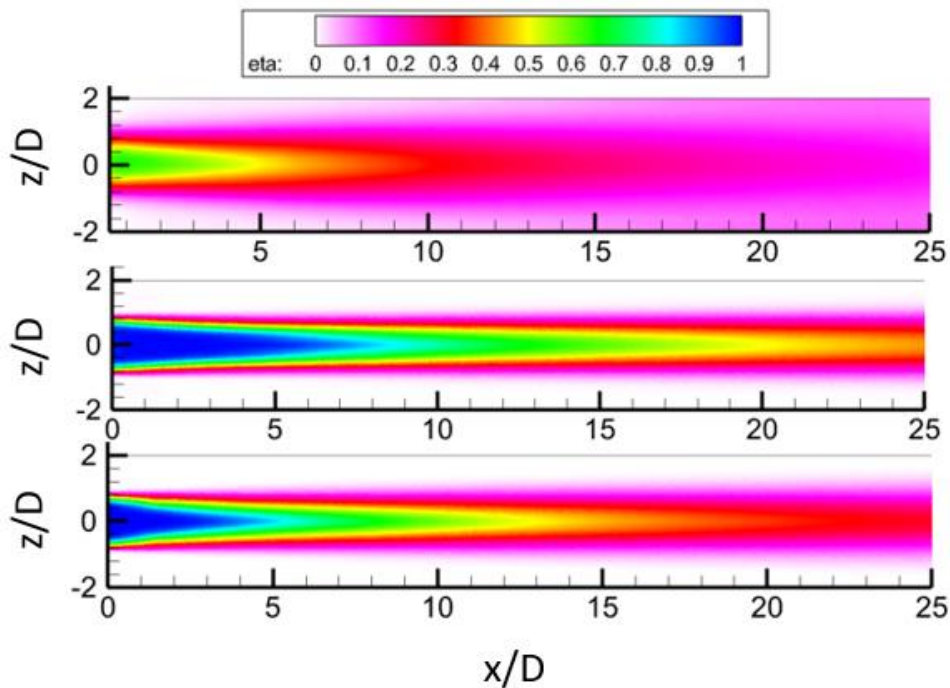


Figure 39  $\eta_{aw}$   $BR=0.5$  comparing experiment (top),  $SST k - \omega$  (middle) and  $k - \epsilon$  (bottom)

Figures 40 and 41 also show the local adiabatic effectiveness for  $BR = 1.0$  and  $BR = 1.5$ , even though the maps are very similar to each other as can also be seen from the results of laterally averaged effectiveness plotted in Figure 38.

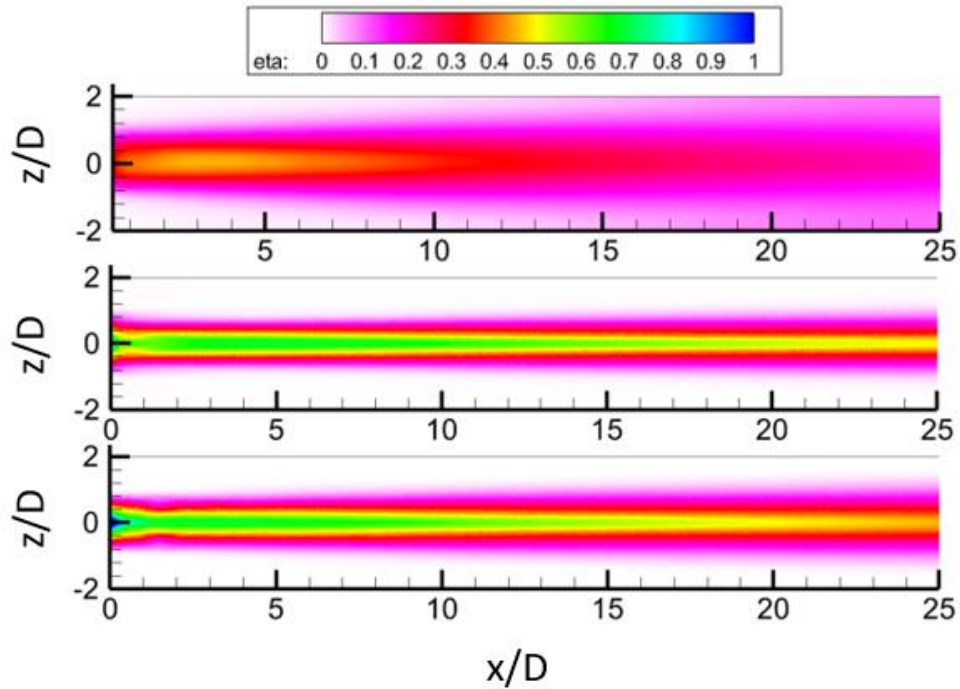


Figure 40  $\eta_{aw}$   $BR=1.0$  comparing experiment (top), SST  $k - \omega$  (middle) and  $k - \epsilon$  (bottom)

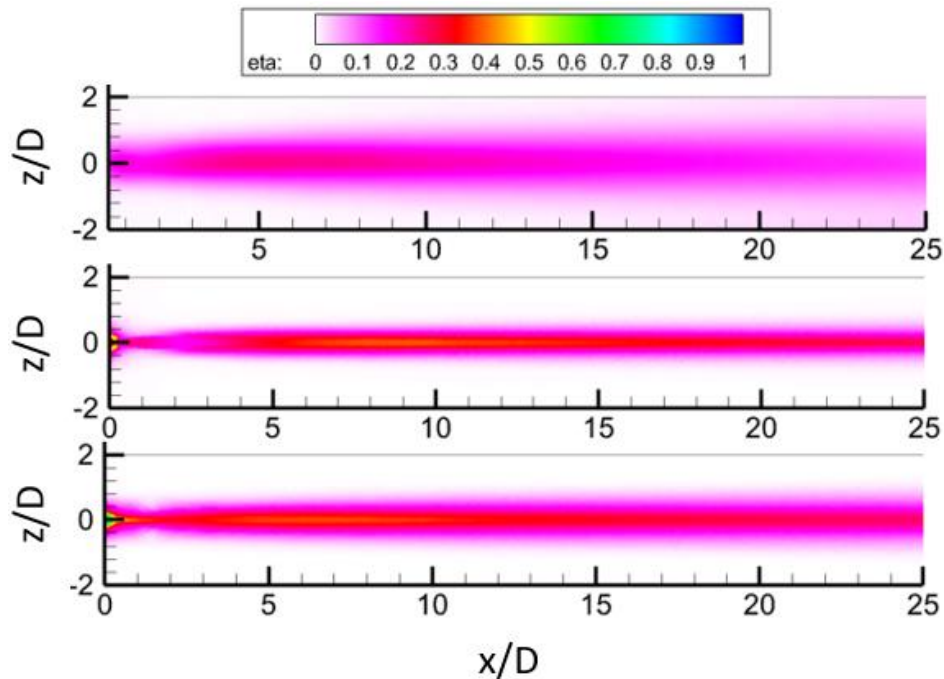


Figure 41  $\eta_{aw}$   $BR=1.5$  comparing experiment (top), SST  $k - \omega$  (middle) and  $k - \epsilon$  (bottom)

To complete the comparison, the channel sections representing the Mach number are presented in Figure 42. There is not much to say, the coolant develops in the same way at the three levels of blowing ratio, clearly the big difference is that having a reduce flow of coolant the velocity inside the channel is reduced for low value of blowing ratio and it increases for high blowing ratio, reaching velocity very close to the speed of sound, thus almost reaching  $Ma = 1$  at the inlet hole in correspondence of the sharp curve the coolant has to do in order to enter the channel. As it will be reported in the next comparison, when the fillet radius effect will be investigated, this high Mach will be reduced increasing the fillet radius, and on the contrary, this region will increase as the radius tends to zero. However this part will be discussed better in the next and last section of this thesis.

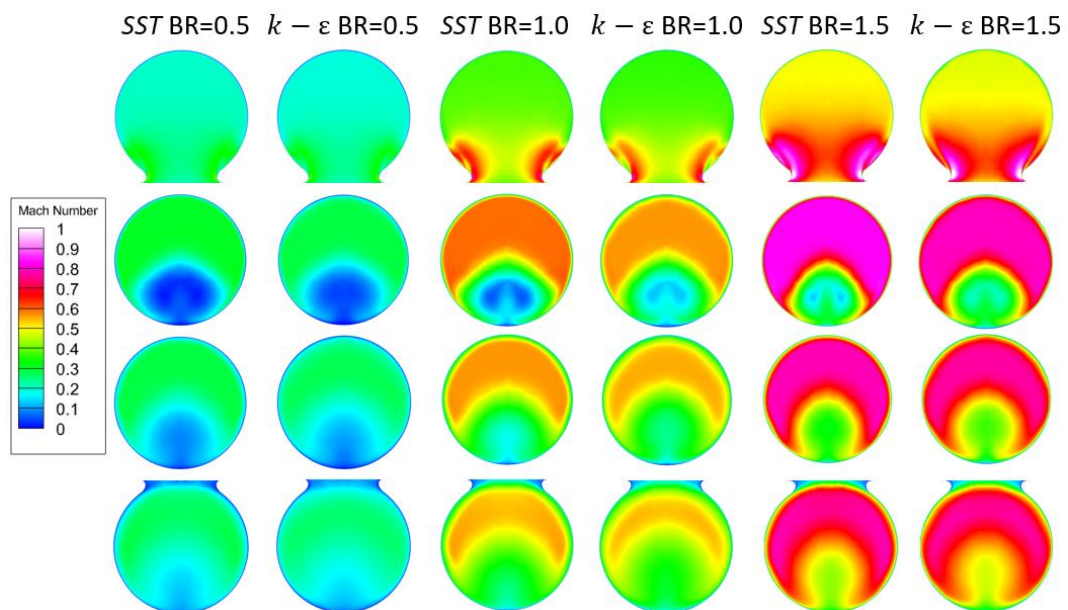


Figure 42 Mach number channel sections

Overall, both turbulence models give a good solution. Poor prediction close to the ejection position of the coolant that can overestimate up to 60% the experimental value for low blowing ratio. On the contrary, for higher values of downstream coordinate a very small discrepancy with respect to the experimental data is obtained. Moreover, independently on the blowing ratio, lateral spread of the numerical solutions is much lower compared to

the experimental maps, making sure the coolant is able to cover a much higher surface area, covering the full lateral extension of the plate surface between two film cooling holes.

The next and final step of this work is the investigation of the fillet radius effect on the film cooling effectiveness. This investigation is carried out considering as turbulence model the *SST k –  $\omega$*  and the analysis is done at the three levels of blowing ratio.

## 6.4 Fillet radius effect

Simulations at three levels of blowing ratio for a single geometry have been compared. Film cooling effectiveness, as resulted from previous investigations, changes greatly if the geometry has the sharp edge or the fillet at the channel edges. For this reason, it has been decided to investigate more thoroughly the impact the fillet radius has on the film cooling performance, concerning local effectiveness maps and laterally averaged effectiveness curves.

A list of fillet radii is presented in order to introduce the simulations that have been run. All the fillet radii reported have been simulated using the *SST k –  $\omega$*  turbulence model and results are compared at three levels of blowing ratio:  $BR = 0.5$ ,  $BR = 1.0$  and  $BR = 1.5$ .

*Sharp Edge*

$$R = 1.25\% D$$

$$R = 2.5\% D$$

$$R = 3.75\% D$$

$$R = 5\% D$$

$$R = 7.5\% D$$

$$R = 10\% D$$

$$R = 15\% D$$

A couple of things have to be explained before introducing the investigation and the results obtained. To begin with, the fillet is built in correspondence

of the edges between the channel and the plenum wall and cooled surface. Fillet radii between 0% (sharp edge) and 5% have been changed both at the inlet and outlet edges of the channel, whereas for fillets higher than 5% the channel diameter, only the inlet edge has been changed keeping the outlet edge constant to 5% the hole diameter. This has been done thinking in a more realistic way, because in a real turbine blade a certain quality of the surface has to be achieved, respecting certain conditions, which means that applying a fillet with a too big radius would be an invasive process that may ruin the desired characteristics of the surface.

Secondly, all the geometries have been simulated with the same inlet total pressure of the coolant. The first simulations to run were those with the 5% fillet radius since previously investigated when comparing the results at different blowing ratios. This means that the pressure used to obtain the correct non-dimensional parameter is set to be appropriate for the 5% case, which means that maintaining the same inlet pressure condition also for the other geometries will result in different non-dimensional parameters. The tuning of the inlet coolant total pressure should be done in order to obtain the proper blowing ratios.

Now that a premises on the simulations conditions has been done, it is time to present and analyse the results obtained with different fillet radii.

Figures [43](#) and [44](#) report the laterally averaged and the local effectiveness results respectively at  $BR = 0.5$ . Except the sharp edge condition all the other results overestimate the experimental data, in particular close to the ejection position where the maximum error is predicted and from the local effectiveness maps it is clear why, the numerical solutions foresee a better coverage of the coolant in proximity of the outlet section downstream the hole. Decreasing the fillet radius to a point where there is no fillet, the coolant coverage decreases, even though a higher effectiveness is predicted anyway.

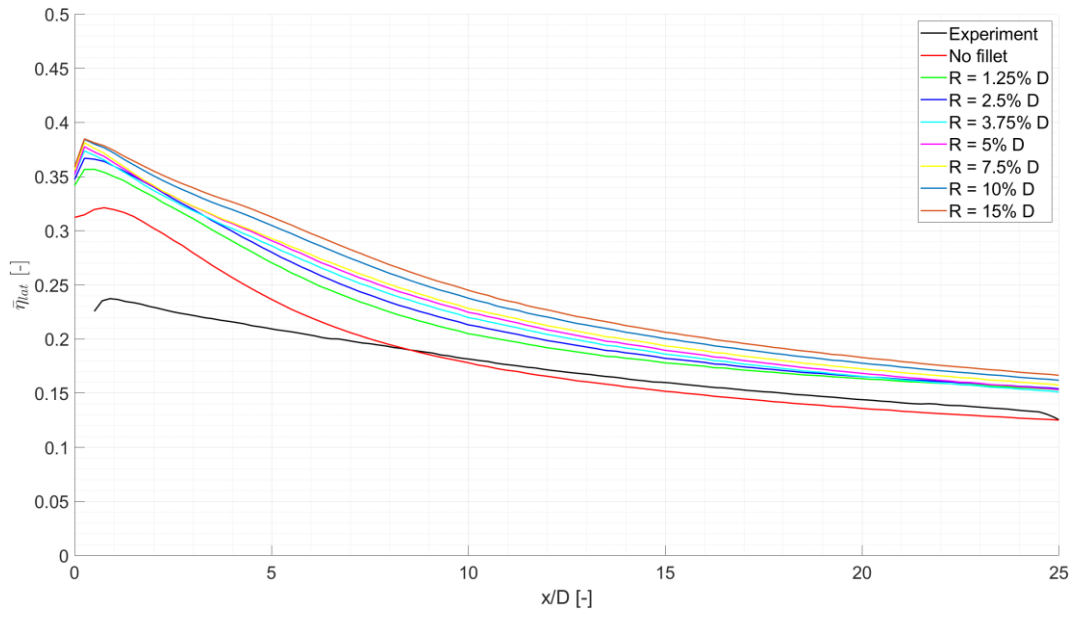


Figure 43 Laterally averaged effectiveness  $BR=0.5$

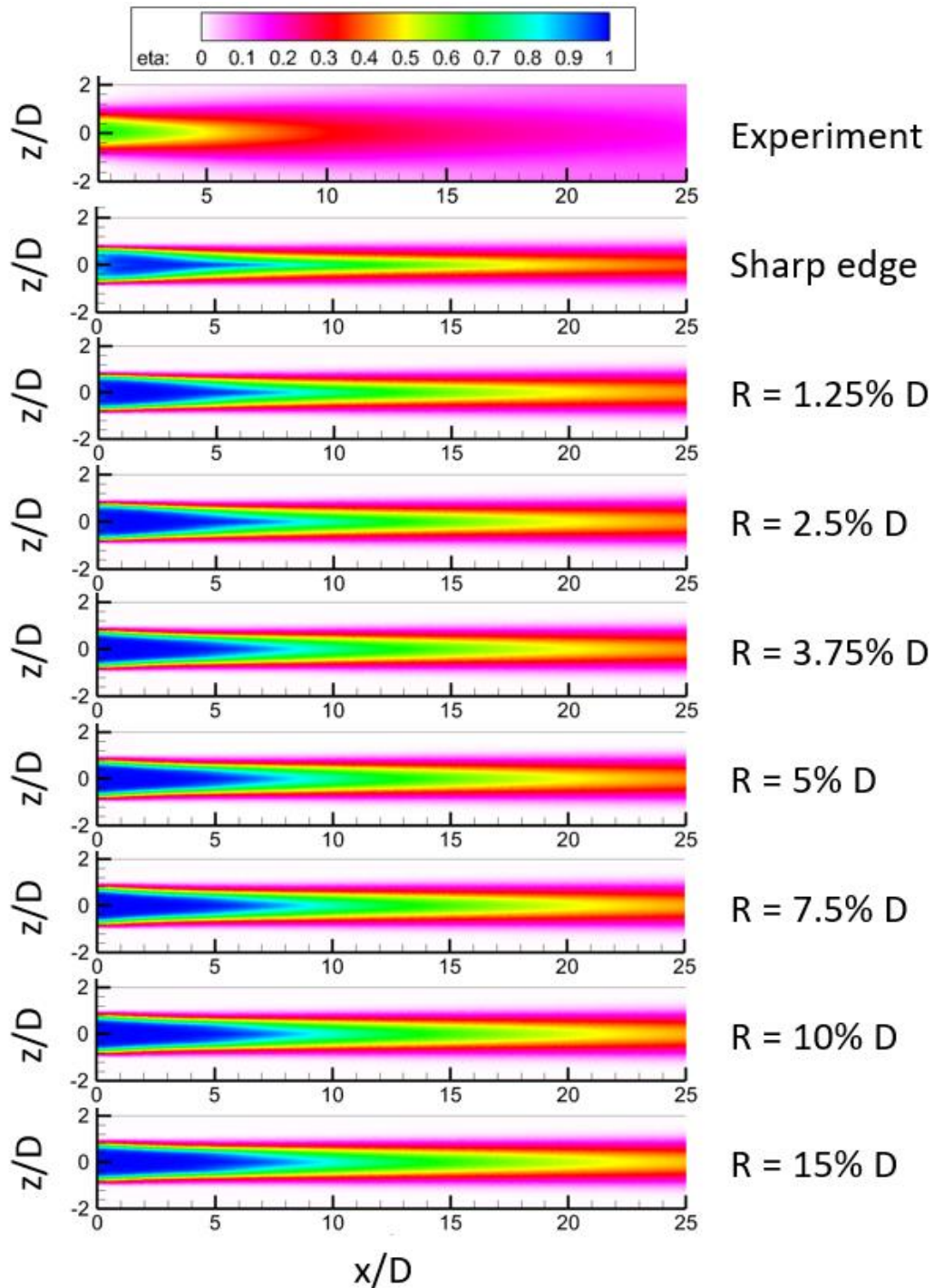
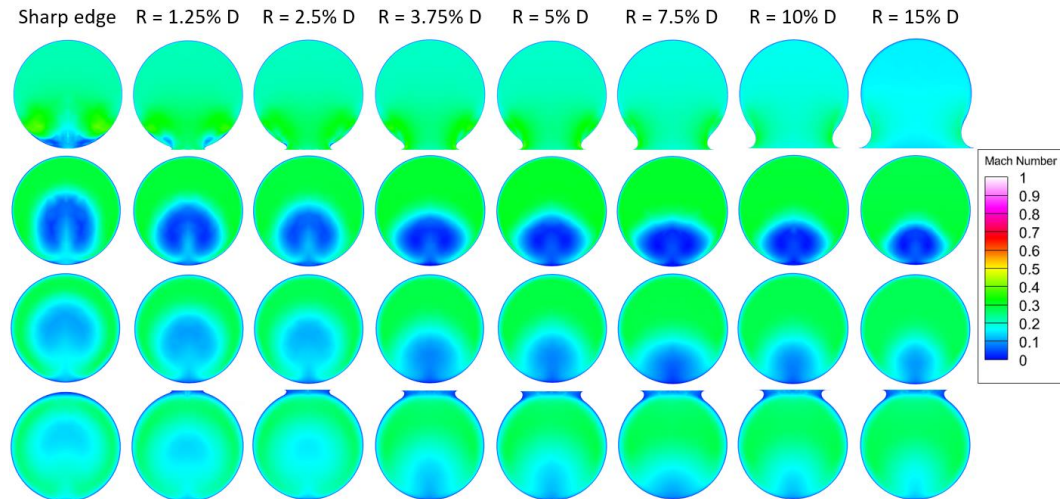


Figure 44 Local adiabatic effectiveness  $BR=0.5$

The results change not only when the effectiveness is compared but also the development of the coolant in the hole changes accordingly to the fillet radius applied. As show in Figure 45 it is evident that increasing the fillet radius, the low velocity region is moved closer to the wall of the channel and it gets smaller and smaller, giving more space to the coolant to flow with

less resistance. this differences are more evident for the case at  $BR = 1.0$  shown in Figure 46, where the velocities are greater, hence the change in Mach is more visible.



*Figure 45 Mach number inside the hole at  $BR=0.5$*

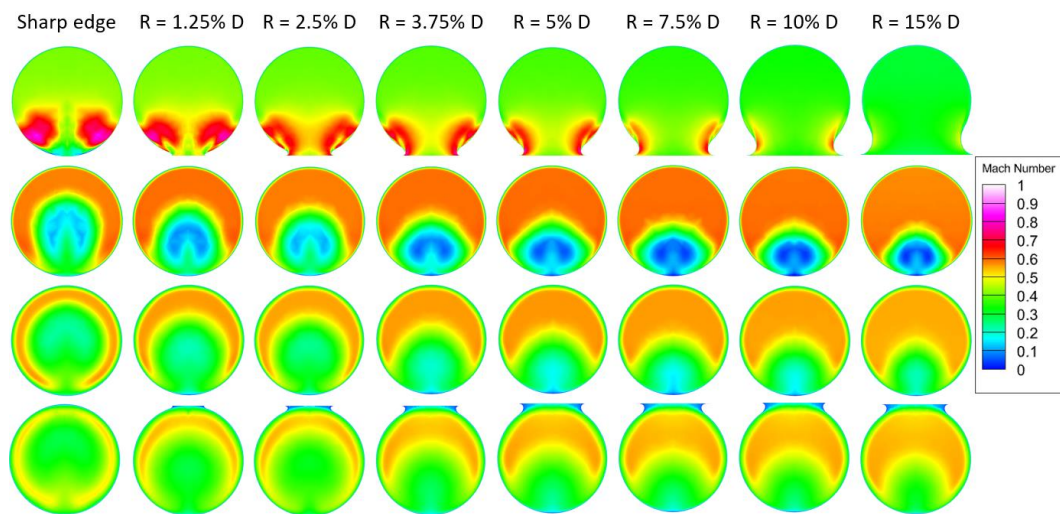


*Figure 46 Mach number inside the hole at  $BR=1.0$*

From Figure 46 it is clearer also how the coolant enters the hole. With the sharp edge geometry the coolant struggles to enter the channel, region with high Mach number is bigger leading to a significant detachment of the coolant from the wall. Increasing the inlet fillet radius, the coolant finds less and less resistance to enter the hole, the fillet helps the coolant to turn, thus the high velocity region at the entrance becomes smaller and smaller, eventually disappearing at  $R = 15\% D$ .

Regarding the results obtained at  $BR = 1.0$ , Figures 47 and 48 report the effectiveness results.  $\bar{\eta}_{lat}$  curves show that most of the solutions underestimate the experimental data downstream the hole, only for low values of fillet radius, smaller than 5%, the results overestimate the experimental data up to  $x/D \sim 10$ . Looking at both  $\bar{\eta}_{lat}$  and  $\eta_{aw}$  the solutions that seem to give better prediction of the results are the 1.25% and 2.5% cases.

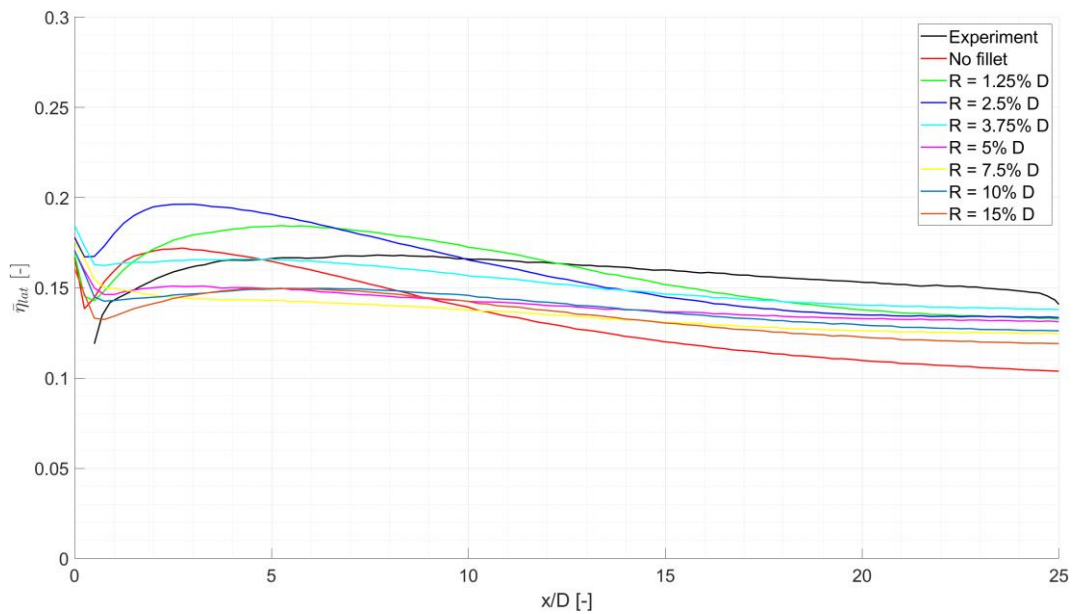


Figure 47 Laterally averaged effectiveness  $BR=1.0$

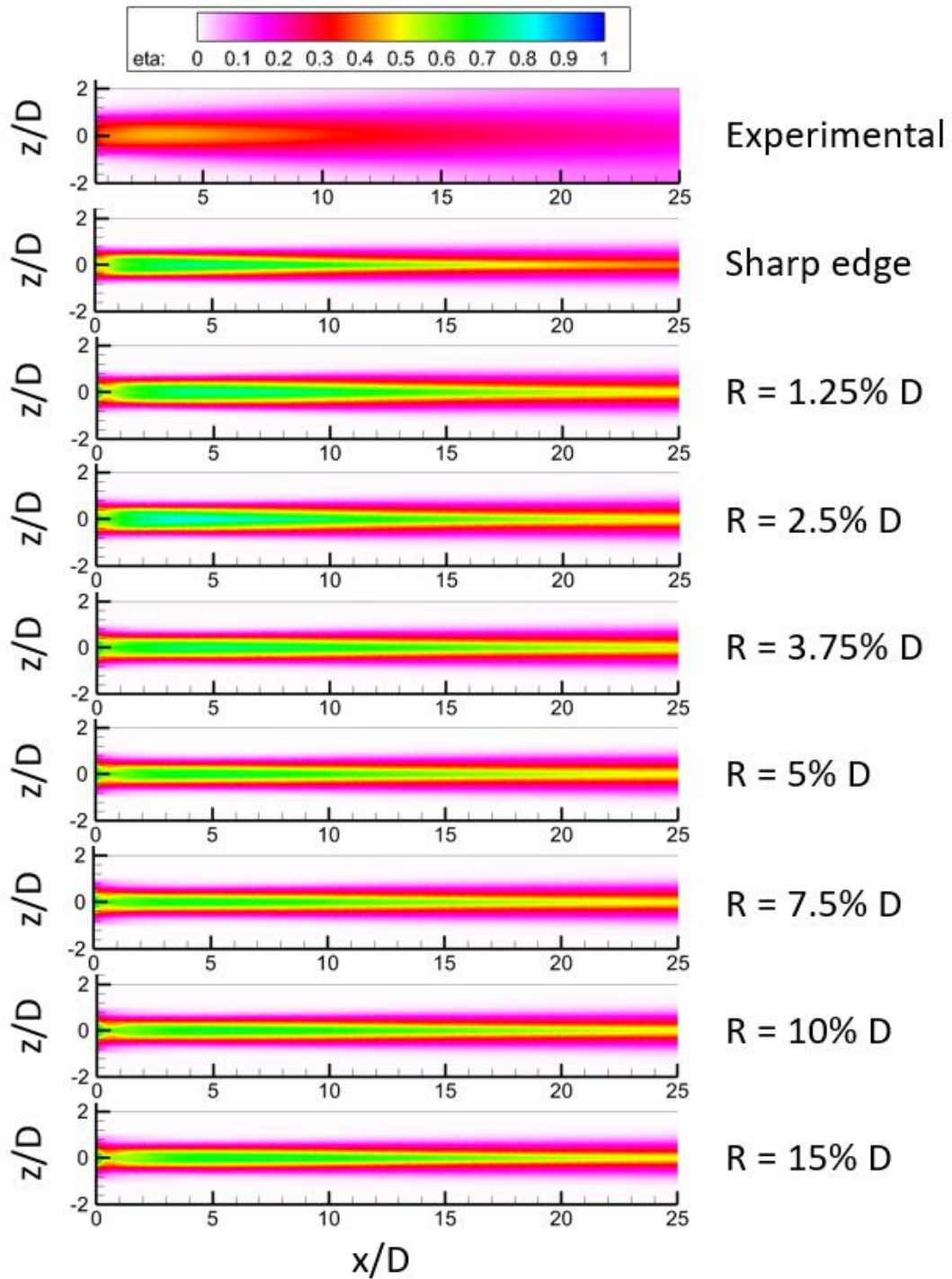


Figure 48 Local adiabatic effectiveness  $BR=1.0$

Lastly, results at  $BR = 1.5$  are compared in Figure 49 and 50 with channel sections representing the Mach number in Figure 51. All the results underestimate the experimental curve with maximum error of about 100% with respect to the experimental data. As for the case at unitary blowing ratio, the best prediction of the results is obtained with the fillet radii of 1.25%

and 2.5% since a better local effectiveness along the centreline of the hole is foreseen.

Sections of the channel representing the Mach number in Figure 51 are not really different from the other two blowing ratio cases, except that the range of velocities is higher compared to the other cases.  $Ma = 1$  is seen at the inlet section of the hole for the geometry without fillet, and it tends to decrease as the fillet radius increases. Bigger radii reduce the flow resistances, thus allowing the coolant to enter easier with less buildup of losses.

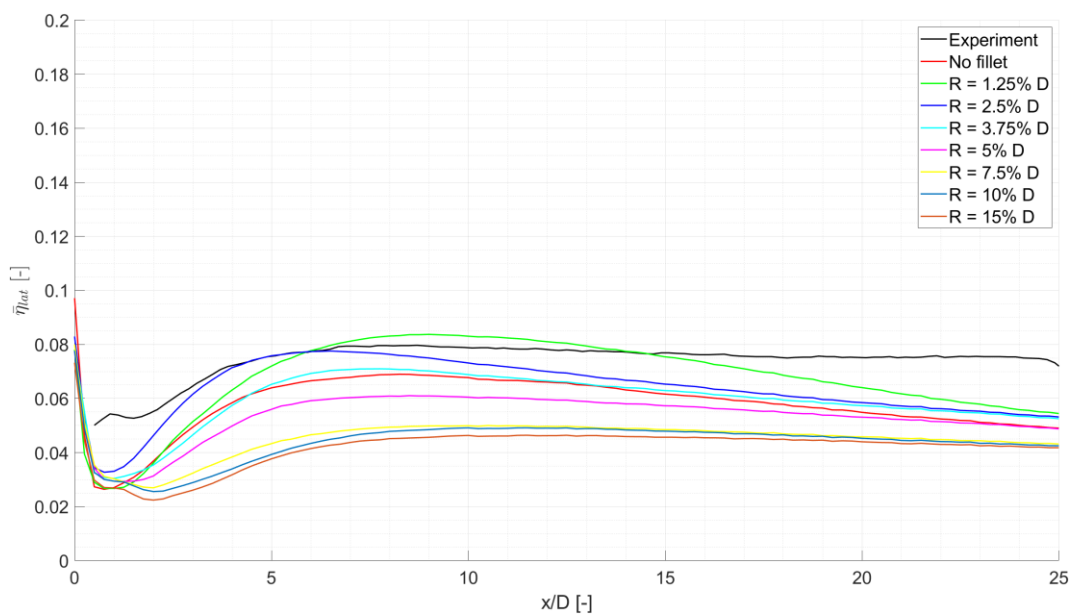


Figure 49 Laterally averaged effectiveness  $BR=1.5$

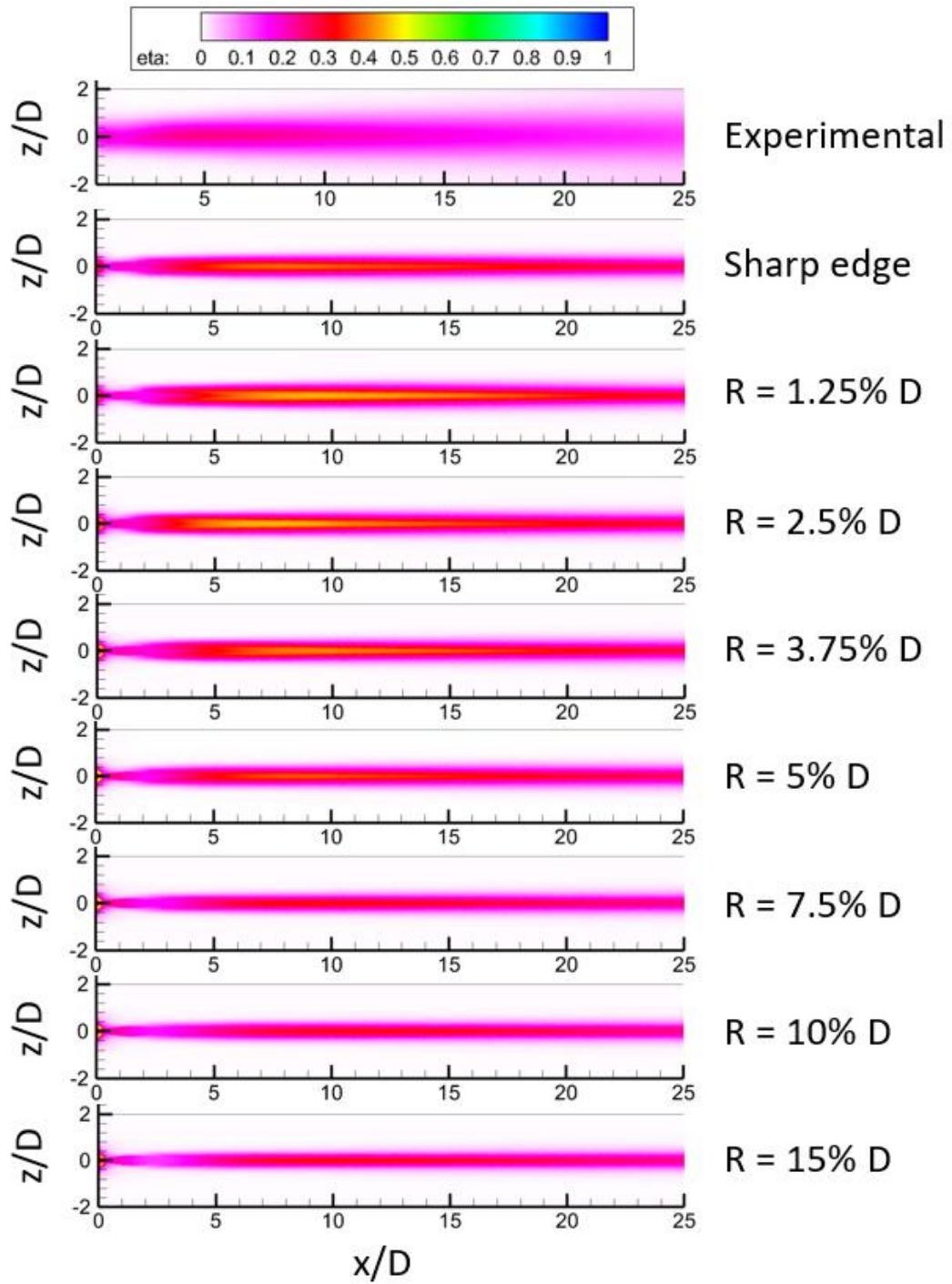


Figure 50 Local adiabatic effectiveness BR=1.5

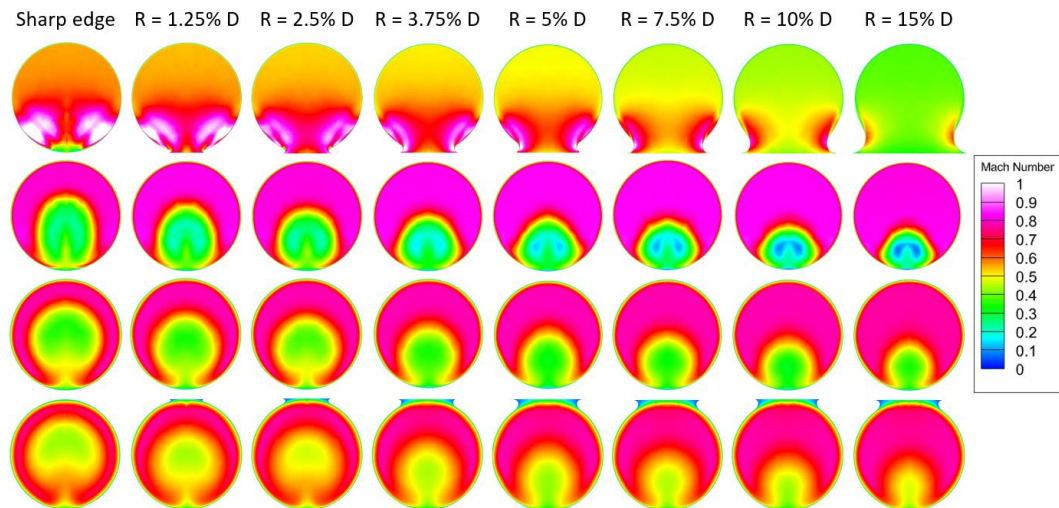


Figure 51 Mach number inside the hole at  $BR=1.5$

Following, in Figure 52, three Mach number maps at  $BR = 1.0$  are reported, presenting respectively the results for sharp edge, 5% fillet and 15% fillet. These three geometrical cases have been selected in order to try to highlight better the differences between the simulations. In accordance with what has been said, the difference in coolant development throughout the hole lays on how the fluid enters the channel. No fillet radius enhances the detachment of the coolant obtaining a low velocity region in the centre of the channel, leading to a more difficult passage of the coolant, while increasing the fillet radius the detachment of the coolant is more and more reduced obtaining a larger region for the coolant to pass.

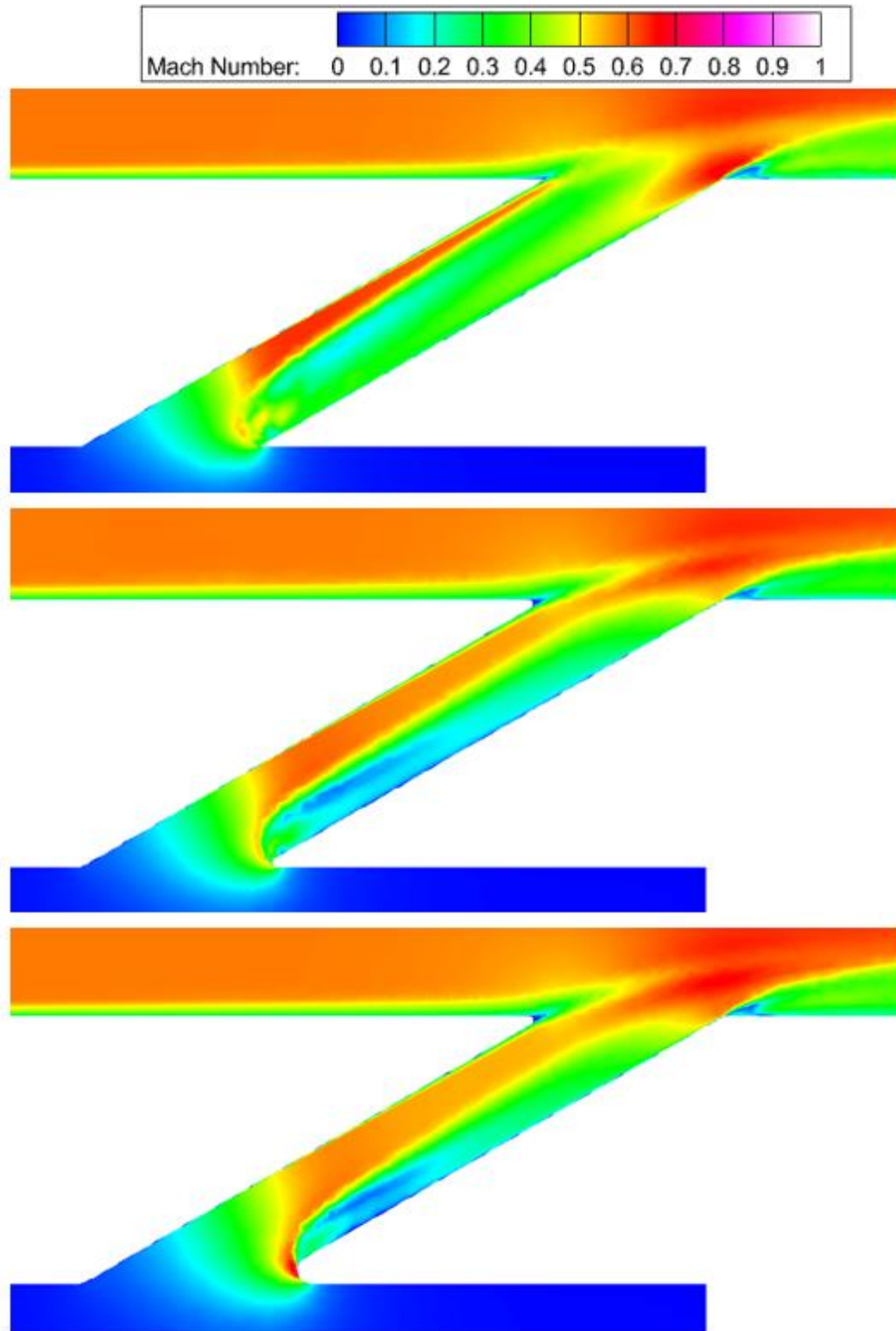


Figure 52 Mach number at  $BR=1.0$  for sharp edge (top), 5% radius (middle) and 15% radius (bottom)

To summarise, the fillet radius has a large impact on the film cooling performance. According to the level of blowing ratio tested, the fillet radius

has different effects on the results. At  $BR = 0.5$  reducing the radius the effectiveness reduces and this is in complete agreement with the sections perpendicular to the channel axis analysed. Decreasing the fillet radius increases the flow losses, most of them obtained at the inlet section of the hole, which eventually impact the coverage of the film cooling layer.

At  $BR = 1.0$ , as for smaller blowing ratio, the losses increase reducing the fillet radius, but in this case there is not a consistent decrement of the effectiveness along all the downstream length decreasing the radius. Close to the ejection position the 2.5% case seems to be the case predicting the highest effectiveness and reducing even more the fillet radius decreases the effectiveness as expected due to higher losses, however differently from the previous case, now the effectiveness is reduced even more if the radius is increased. Based on what has been said before, the effectiveness should increase because the losses are reduced, but considering that the blowing ratio is a value high enough to make the coolant to start lifting off from the surface, the reduced losses derived from an increment of fillet radius give the coolant flow more capability to penetrate the mainstream slightly reducing its performance.

At  $BR = 1.5$ , where the lift-off of the coolant is dominant, increasing the fillet radius greatly reduces the film cooling effectiveness. This behaviour of the curves, where the effectiveness is reduced increasing the fillet radius is due to the fact that, as said at the beginning of this part of the investigation, the inlet coolant total pressure has not been modified for all the geometrical cases, hence the desired non-dimensional parameter is not met. In this way, the case with  $BR = 1.5$  will actually result in having blowing ratios greater or smaller depending on if the fillet radius is increased or decreased.

This same explanation is applicable at  $BR = 0.5$ , but in this case the increase or reduction of the actual blowing ratio gives results completely opposite to what has been obtained at  $BR = 1.5$ . In this case, since all the curves overestimate the experimental data, if the fillet radius is reduced the blowing ratio will decrease and the losses will increase resulting in a lower effectiveness that is closer to the experimental curve.

Following, Table 5 with the blowing ratio values for each fillet radius case is reported.

	<b><i>BR = 0.5</i></b>	<b><i>BR = 1.0</i></b>	<b><i>BR = 1.5</i></b>
<b><i>Sharp Edge</i></b>	0.43	0.92	1.37
<b><i>R = 1.25% D</i></b>	0.46	0.95	1.43
<b><i>R = 2.5% D</i></b>	0.47	0.96	1.45
<b><i>R = 3.75% D</i></b>	0.48	1.00	1.49
<b><i>R = 5% D</i></b>	0.50	1.00	1.50
<b><i>R = 7.5% D</i></b>	0.50	1.05	1.55
<b><i>R = 10% D</i></b>	0.51	1.07	1.58
<b><i>R = 15% D</i></b>	0.53	1.11	1.63

Table 5 Blowing ratios at different fillet radius conditions

## 7 Discharge coefficient $C_D$

Predictions of the discharge coefficient are compared with the experimental results in an equivalent set up condition, the only difference is the hole diameter that is double the diameter used for numerical solutions of the problem. All the other operating conditions are the same.

Figure [53](#) reports the graph with the experimental and numerical results of  $C_D$ . The values shown are obtained at different geometrical conditions for each fillet radius used. This graph is the most complete and contains the discharge coefficient values at each blowing ratio tested. As for when the comparison of effectiveness results has been done, also the discharge coefficients are compared using the *SST*  $k - \omega$  as turbulence model.

Results show both an underprediction and an overprediction of the experiments the discharge coefficient increases as the fillet radius increases, because a higher radius allows the coolant to enter the hole with more ease and the losses are reduced. The change between underestimation to overestimation occurs at approximately 2.5% the channel diameter. Based on the results obtained this case seems to be the best to predict the losses compared to the data experimentally obtained.

As said before, the inlet coolant total pressure is correct only for the 5% case, all the other simulations maintain the same pressure conditions, hence the non-dimensional parameter as the blowing ratio slightly change, and the discharge coefficient changes accordingly, so the values obtained may not be the precise values that can be numerically obtained.

Globally, the presence of the filleted edge helps the flow turning and entering the coolant channel, resulting in lower fluid losses at the entrance of the channel.

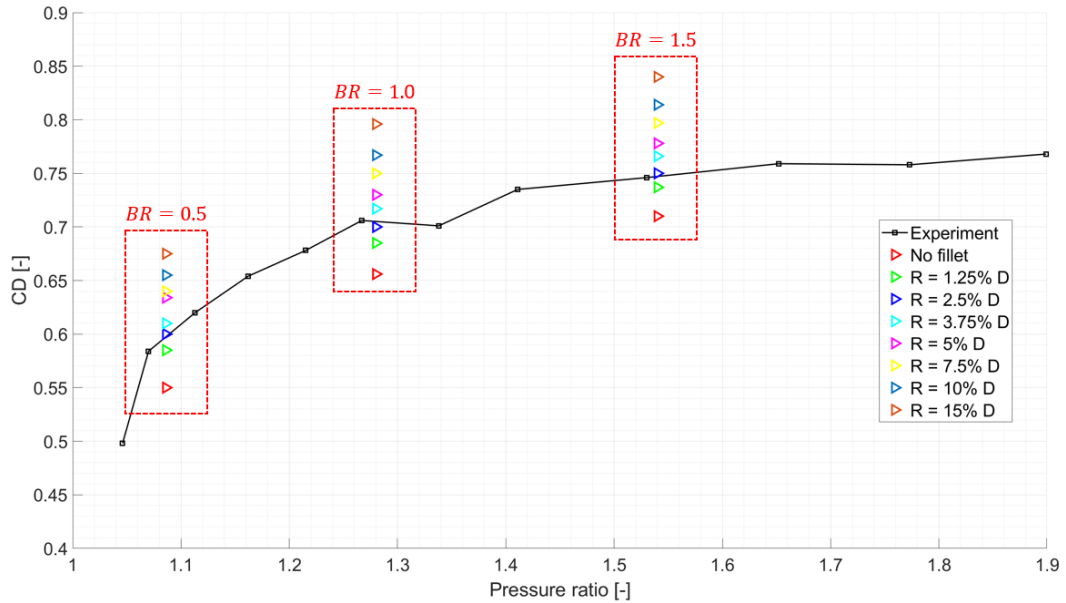


Figure 53 Discharge coefficient

As for Table 5, in Table 6 are reported the discharge coefficient values for every fillet radius at each blowing ratio condition.

	<b>BR = 0.5</b>	<b>BR = 1.0</b>	<b>BR = 1.5</b>
<b>Sharp Edge</b>	0.55	0.66	0.71
<b>R = 1.25% D</b>	0.59	0.69	0.74
<b>R = 2.5% D</b>	0.60	0.70	0.75
<b>R = 3.75% D</b>	0.61	0.72	0.77
<b>R = 5% D</b>	0.63	0.73	0.78
<b>R = 7.5% D</b>	0.64	0.75	0.80
<b>R = 10% D</b>	0.66	0.77	0.81
<b>R = 15% D</b>	0.68	0.80	0.84

Table 6 Discharge coefficients

## 8 Conclusions and future development

The presented work has been carried out in collaboration with Avio Aero, that include a numerical Steady RANS investigation on the film cooling system of HPT stages. Aero-thermal performance of film cooling has been studied, analysing both film cooling effectiveness and discharge coefficient as results, comparing numerical solutions to experimental results.

To begin with, a general overview on the working principle of a turbojet engine has been done to introduce the topic and have a better idea where and why it is necessary to have a good cooling system.

Following, the film cooling phenomenon itself has been briefly explained, presenting why it is necessary to have such an advanced cooling system and introducing the main complexities found in the developing of such system.

Once the topic has been broadly introduced, a description of the actual work has been brought on, introducing step by step the working process at last leading to the discussion of the final results.

First simulations have been run to identify the proper grid structure to use in the next steps for the rest of the project. Tetrahedral and polyhedral meshes have been tested and a grid sensitivity analysis on both has been performed. The tetrahedral mesh with approximately slightly more than three million elements has been decided to use. Poor quality of the inflation layer in correspondence of the edges and bad flow structure close to the inlet channel section for the polyhedral mesh were the reason why this mesh was rejected.

Along with the choice of the mesh, the tuning of the inlet coolant pressure to ensure a unitary blowing ratio has been achieved. Simulations at  $BR = 1.0$  were run to understand which two-equation turbulence model use, according to the accuracy of the results based on the experimental data. Standard  $k-\omega$ , SST  $k-\omega$  and standard  $k-\varepsilon$  are the models used. SST  $k-\omega$  and  $k-\varepsilon$  are the models that better represent the experimental solutions. The choice of the turbulence model has been done by comparing results

obtained from a sharp edge conditions and a 5% fillet condition. The sharp edge geometry condition (as it is the experimental setup) was not representing well the experimental results, hence the 5% geometry has been set as default geometry for the next simulations.

Now that the geometry has been selected,  $BR = 0.5$  and  $BR = 1.5$  have been investigated with  $SST k - \omega$  and  $k - \varepsilon$ .  $SST k - \omega$  is the turbulence model that has been decided to use. This investigations did not stop at a 5% fillet radius, but it has been decided to apply it on other geometrical features by changing the fillet radius.

In the end, laterally averaged and local adiabatic film cooling effectiveness and discharge coefficient have been compared with the experimental results. Globally, the use of a steady RANS approach does not result in an accurate prediction of the experimental results. Numerical results tend to overestimate the experimental results for low blowing ratio, while underestimate them at high blowing ratio. An explanation looking at the adiabatic effectiveness maps can be seen, where it is evident that the numerical data simulate a greater coverage of the coolant with respect to the experimental maps, and the lateral distribution of the coolant is greatly reduced. Changing the fillet radius slightly modify the effectiveness maps, however the changes can be more appreciated comparing the  $\bar{\eta}_{lat}$ , where smaller radii happen to give better approximation of the results in particular at higher blowing ratios. This improvement is also captured in the discharge coefficient, where very good prediction of the experiment is obtained for  $R = 2.5\% D$ .

Overall, good prediction of the results has been obtained considering the time and computational efforts required by the software.

Eventually, the application of unsteady simulations or more complete turbulence models, that are able to capture the larger scales of turbulence, might result in an improvement of the numerical accuracy compared to the steady analysis. With a better prediction of what happen at inertial length scale, the mixing of coolant with hot gas, as well as the lateral distribution of coolant over the surface, can be better predicted.

This project investigated on a small fraction of the macro argument regarding the film cooling. Geometrical and fluid properties can be changed to further investigate the film cooling phenomenon. Geometry configurations such as fan-shaped or laidback fan-shaped hole can be adopted, different injection angles can be investigated, and different fluid properties can be varied, such as the main flow and coolant Mach number, or the crossflow conditions for both main flow and coolant. The possible investigations and the possible combinations to analyse are endless and the parameters that influence the film cooling are countless between geometrical, fluid and computational properties.

## **Acknowledgments**

This thesis represents not only my work at the computer, but it is the result of hard work and dedication in doing something the best possible way that really fascinate me. This experience carried out in collaboration with Avio Aero has been a unique opportunity to work with a group of professional and skilled individuals. First and foremost I wish to thank my supervisors at Politecnico di Torino, Professor Daniela Misul, Ing. Simone Salvadori, Dr. Nicola Rosafio and Professor Mirko Baratta who have been supportive and dedicated through the completion of this thesis. A big thank you goes to the supervisors at Avio Aero who allowed me to work with them at the thesis and during my internship: Ing. Daniele Coutandin, Ing. Alberto Buonvino and Ing. Mirko Pavan. All these people I had the opportunity to work with were very professional and available at any time to give me support the best they could. Working with them not only gave the possibility to learn something new, but I also had the opportunity to grow professionally and the relationship I had with the company really contributed to that. A last thank you goes to the Academic Computing service provided by DAUIN (Dipartimento di Automatica e Informatica): Computational resources were provided by HPC@POLITO, a project of Academic Computing within the Department of Control and Computer Engineering at the Politecnico di Torino (<http://www.hpc.polito.it>).

I would like to take this opportunity to thank the person that started all of this, Ing. Alessandro Heltai and Dr. Francesco Macchiaroli, as well as all the people that helped me afterwards: Dr. Luigi Piva, Dr. Mariafrancesca Magoni and Dr. Susanna Posfortunato.

A thank you goes to all my friends with whom I shared ups and downs during these long five years that all condensed to this point. Thank you Giacomo, Giulio, Elisabetta, Stefano, Donato, Corrado and Alessandro.

Last but not least, the final thank you goes to my family who are my source of energy and the people I look up the most, you are truly an example of life

for me. You have never forced me to do something because you believed it was the right thing to do, but rather you encouraged me and let me go my way, suggesting and helping me whenever I found an obstacle. Thank you for believing in me and sacrificing a lot for me.

## **Ringraziamenti**

Questa tesi non rappresenta solo il mio lavoro di fronte ad uno schermo, ma è il risultato di duro lavoro e dedizione nel fare qualcosa nel miglior modo possibile che mi affascina seriamente. Questa esperienza svolta in collaborazione con Avio Aero è stata un'opportunità unica per lavorare con un gruppo di persone altamente professionali ed esperte. Prima di tutti vorrei ringraziare i docenti del Politecnico di Torino che mi hanno seguito in questo lavoro, Prof. Daniela Misul, Ing. Simone Salvadori, Dr. Nicola Rosafio e Prof. Mirko Baratta che mi hanno supportato durante lo svolgimento della tesi. Un grosso grazie va anche al team di Avio Aero, Ing. Daniele Coutandin, Ing. Alberto Buonvino and Ing. Mirko Pavan, con cui ho interagito in questi mesi che mi hanno dato la possibilità di lavorare con loro alla tesi e durante i mesi di tirocinio. Tutte queste persone con cui ho avuto l'opportunità di lavorare sono state molto professionali e disponibili in qualsiasi momento per darmi una mano. Lavorare con loro non solo mi ha dato la possibilità di imparare qualcosa di nuovo, ma ho anche avuto modo di crescere professionalmente e il rapporto che ho avuto con l'azienda durante questi mesi ha contribuito molto. Un ringraziamento anche al DAUIN (Dipartimento di Aeronautica e Informatica): Computational resources were provided by HPC@POLITO, a project of Academic Computing within the Department of Control and Computer Engineering at the Politecnico di Torino (<http://www.hpc.polito.it>).

Vorrei cogliere questo spazio per ringraziare anche le persone che mi hanno permesso di iniziare tutto questo, Ing. Alessandro Heltai e Dr. Francesco Macchiaroli, così come le persone che mi hanno aiutato in seguito, Dr. Luigi Piva, Dott.ssa Mariafrancesca Magoni e Dott.ssa Susanna Posfortunato.

Un grazie va ai miei amici e compagni di corso con i quali ho condiviso alti e bassi durante questi lunghi cinque anni che hanno portato a questo

momento. Grazie Giacomo, Giulio, Elisabetta, Stefano, Donato, Corrado e Alessandro.

Ed infine, ma non per importanza, un grazie va alla mia famiglia che sono la fonte di energia e sono le persone che più ammiro. Siete un vero esempio di vita per me. Non mi avete mai forzato a fare qualcosa perché fosse la cosa giusta da fare, ma piuttosto mi avete incoraggiato e fatto prendere le mie decisioni, supportandomi e aiutandomi nei momenti di difficoltà. Grazie per aver sempre creduto e fatto tanti sacrifici per me.

## References

- [1] Saumweber, C., Schulz, A., Wittig, S., Task C1 – Discharge coefficient correlations for shaped holes. Report No. C1/Karlsruhe/1/ed1, BRITE EURAM PROJECT TATEF CONTRACT BRPR-CT97-0519
- [2] Saumweber, C., Schulz, A., Wittig, S., Task C2 – Lateral interactions of film cooling holes. Report No. C2/Karlsruhe/1/ed1, BRITE EURAM PROJECT TATEF CONTRACT BRPR-CT97-0519
- [3] Salvadori, S., Montomoli, F., Martelli, F., Film cooling performance in supersonic flows: effects of shock impingement. TATEF2
- [4] Baldauf, S., Scheurlen, A., Schulz, A., Wittig, S., Correlation of film cooling effectiveness from thermographic measurements at engine like conditions. ASME 2002; GT2002-30180: 149-162.
- [5] Lutum, E., Johnson, B.V., Influence of the hole length-to-diameter ratio on film cooling with cylindrical holes. *Journal of Turbomachinery* 2005; 121(2): 209-216.
- [6] Zhang, J., Zhang, S., Wang, C., Tan, X., Recent advances in film cooling enhancement: A review. *Chinese Journal of Aeronautics* 2020; 33(4): 1119-1136.
- [7] Argyropoulos, C.D., Markatos, N.C., Recent advances on the numerical modelling of turbulent flows. *Applied Mathematical Modelling* 2015; 39(2): 693-732.
- [8] Rosafio, N., Salvadori, S., Misul, A. D., Baratta, M., Carnevale, M., Saumweber, C., Effect of self-sustained pulsation of coolant flow on adiabatic effectiveness and net heat flux reduction on a flat plate. ASME 2021; GT2021-59663.